Geophysical Journal International

Geophys. J. Int. (2015) **201,** 1912–1938
GJI Geodynamics and tectonics

doi: 10.1093/gji/ggv102

Crustal structure of the eastern Algerian continental margin and adjacent deep basin: implications for late Cenozoic geodynamic evolution of the western Mediterranean

B. Bouyahiaoui,[1] F. Sage,[2] A. Abtout,[1] F. Klingelhoefer,[3] K. Yelles-Chaouche,[1] P. Schnürle,[3] A. Marok,[4] J. Déverchère,[5] M. Arab,[6] A. Galve[2] and J.Y. Collot[2]

[1]*Centre de Recherche en Astronomie, Astrophysique et Géophysique (CRAAG), BP* 63 *Bouzaréah* 16340 *Alger, Algérie. E-mail: b.bouyahiaoui@yahoo.com*
[2]*UMPC, UNSA, CNRS, IRD, Géoazur,* 250, *Avenue Albert Einstein, F*-06560 *Valbonne, France*
[3]*Institut Français de Recherche pour l'Exploitation de la Mer (IFREMER), ZI de la Pointe de Diable, F*-29280 *Plouzané, France*
[4]*Department of Earth and Universe Sciences, University of Tlemcen, BP* 119, 13000 *Tlemcen, Algeria*
[5]*Université de Brest (UBO), CNRS UMR*6538 *Domaines Océaniques, Institut Universitaire Européen de la Mer, F*-29280 *Plouzané, France*
[6]*Sonatrach Exploration, Algerian National Oil Company, Algeria*

Accepted 2015 February 26. Received 2015 February 25; in original form 2014 June 30

SUMMARY

We determine the deep structure of the eastern Algerian basin and its southern margin in the Annaba region (easternmost Algeria), to better constrain the plate kinematic reconstruction in this region. This study is based on new geophysical data collected during the SPIRAL cruise in 2009, which included a wide-angle, 240-km-long, onshore–offshore seismic profile, multichannel seismic reflection lines and gravity and magnetic data, complemented by the available geophysical data for the study area. The analysis and modelling of the wide-angle seismic data including refracted and reflected arrival travel times, and integrated with the multichannel seismic reflection lines, reveal the detailed structure of an ocean-to-continent transition. In the deep basin, there is an ∼5.5-km-thick oceanic crust that is composed of two layers. The upper layer of the crust is defined by a high velocity gradient and *P*-wave velocities between 4.8 and 6.0 km s^{-1}, from the top to the bottom. The lower crust is defined by a lower velocity gradient and *P*-wave velocity between 6.0 and 7.1 km s^{-1}. The Poisson ratio in the lower crust deduced from *S*-wave modelling is 0.28, which indicates that the lower crust is composed mainly of gabbros. Below the continental edge, a typical continental crust with *P*-wave velocities between 5.2 and 7.0 km s^{-1}, from the top to the bottom, shows a gradual seaward thinning of ∼15 km over an ∼35-km distance. This thinning is regularly distributed between the upper and lower crusts, and it characterizes a rifted margin, which has resulted from backarc extension at the rear of the Kabylian block, here represented by the Edough Massif at the shoreline. Above the continental basement, an ∼2-km-thick, pre-Messinian sediment layer with a complex internal structure is interpreted as allochthonous nappes of flysch backthrusted on the margin during the collision of Kabylia with the African margin. The crustal structure, moreover, provides evidence for Miocene emplacement of magmatic intrusions in both the deep basin and the continental margin. Based on the crustal structure, we propose that the eastern Algerian basin opened during the southeastward migration of the European forearc before the collision, along a NW–SE elongated spreading centre that ran perpendicular to the subduction trend. Such an atypical geometry is explained by the diverging directions of the subduction rollback during the backarc opening: eastward for the Corsica–Sardinia block, and southward for the Kabylian blocks. This geometry of the forearc can be interpreted as the surface expression of a slab tear at depth, which is responsible for atypical magmatism in the overlying backarc oceanic basin.

Key words: Tomography; Composition of the oceanic crust; Continental margins; divergent; Africa.

1 INTRODUCTION

The Mediterranean Sea at present forms a single, 2.5 × 10^6 km^2 basin that is surrounded by continents. However, in further detail, it is composed of a complex mosaic of sub-basins that show different ages and different evolutionary stages, which mark out the Africa–European convergent boundary. While some of these sub-basins are ancient oceans that closed along active subduction zones, such as the eastern Mediterranean basin (e.g. Dercourt *et al.* 1986; Wortel & Spakman 2000; Jolivet *et al.* 2003), some others are still opening, such as the Tyrrhenian basin (e.g. Gueguen *et al.* 1998; Sartori *et al.* 2001; Rosenbaum & Lister 2004a), or opened during the Oligo-Miocene, such as the Liguro-Provençal basin or the Algerian basin (e.g. Bouillin 1986; Faccenna *et al.* 2001; Rosenbaum *et al.* 2002; Gattacceca *et al.* 2007; Billi *et al.* 2011; Sage *et al.* 2011; Fig. 1a). The Mediterranean basin is, moreover, surrounded by orogenic belts that attest to the Cenozoic closure of the oceans that were previously part of the Mediterranean domain. Rapid transition in time and in space from basin opening at the back of the subduction zones to collision zones has characterized the African–Eurasian border for at least 50 Ma (e.g. Jolivet *et al.* 2003), which led to the present-day Mediterranean configuration. Understanding the spatiotemporal

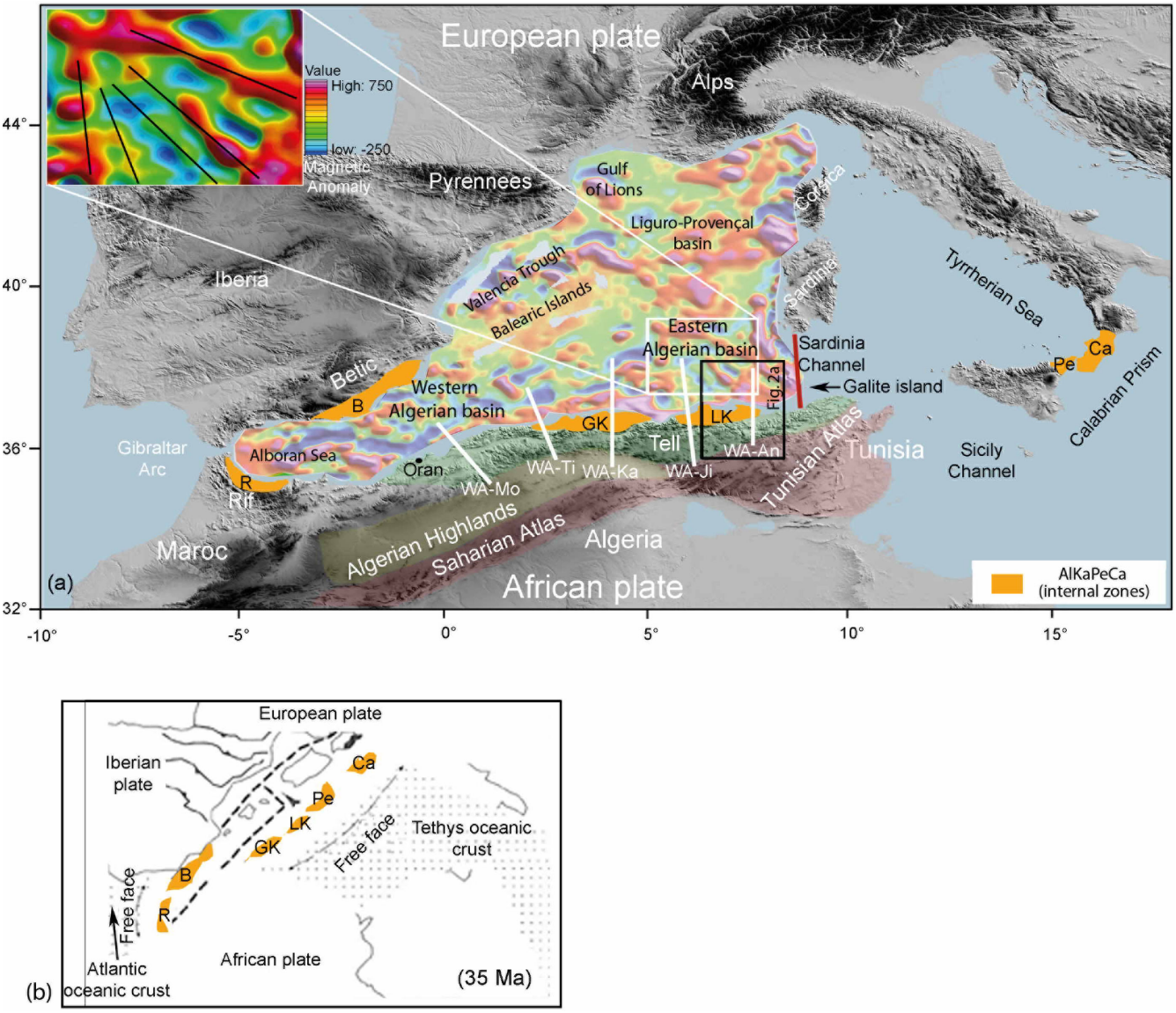

Figure 1. (a) Magnetic anomalies from Galdeano & Rossignol (1977) superimposed on the map of the Western Mediterranean area. White lines: location of the five wide-angle seismic profiles acquired during SPIRAL cruise. WA-An, Annaba profile (this study); WA-Ji, Jijel profile; WA-Ka, Great Kabylia profile; WA-Ti, Tipaza profile and WA-Mo, Mostaganem profile. Red line: location of the wide-angle seismic profile from the European Geotraverse project (Peirce & Barton 1992). White frame: location of the inset that displays regularly organized NW–SE magnetic anomalies in the central part of the eastern Algerian basin (from Schettino & Turco 2006). Black frame: location of the central eastern Algerian basin as displayed in Fig. 2. (b) Western Mediterranean setting at 35 Ma, modified from Gelabert *et al.* (2002), indicating the location of the European forearc (in yellow), before the Algerian basin opening. During the Algerian and Tyrrhenian basin formation, the European forearc was fragmented and migrated to the south and to the east to reach its present day position (shown in (a)), due to subduction rollback (see text for details and references). The names of the forearc fragments were given according to their present-day location, and are from west to east: R, Rif; B, Betics; GK, Great Kabylia; LK, Lesser Kabylia; Pe, Peloritani; Ca, Calabria. They form the AlKaPeCa block defined by Bouillin (1986), with Al, Alboran = R+B; Ka, Kabylia = GK+PK; Pe, Peloritani and Ca, Calabria.

evolution of the Mediterranean basins is important, to be able to better unravel the process of backarc opening and the evolution of complex convergent plate boundaries.

Numerous kinematic models have been proposed to explain the current structure of the western Mediterranean basin that have mostly been based on magnetic data (Schettino & Turco 2006; Gattacceca *et al.* 2007), crustal structures of the basin and adjacent margins (Mauffret *et al.* 2004), geological observations of the Mediterranean collision zone (Lustrino *et al.* 2011; Carminati *et al.* 2012), kinematic constraints (Gueguen *et al.* 1998; Jolivet & Faccenna 2000) and the integration of different types of data (e.g. tectonic, seismological, geodetic, tomographic, seismic reflection data; Billi *et al.* 2011). All of the kinematic reconstruction models agree that in an initial stage before the opening of the Algerian basin, the Alboran, Kabylia, Peloritani and Calabria blocks, which were defined as the AlKaPeCa block (Bouillin 1986), were part of the European southern margin until ∼23 Ma (Alvarez *et al.* 1974; Cohen 1980; Bouillin 1986; Lonergan & White 1997; Vergés & Sabàt 1999; Frizon de Lamotte *et al.* 2000; Rosenbaum *et al.* 2002; Mauffret *et al.* 2004; Billi *et al.* 2011). The kinematic reconstruction models also agree that in a final stage, the AlKaPeCA blocks accreted by collision along the northern African border, ∼16–18 Ma (Fig. 1a, R, GK, LK) (Monié *et al.* 1984; Saadallah & Caby 1996; Lonergan & White 1997; Faccenna *et al.* 2001; Roure *et al.* 2012), the collision zone being underlain by a detached, northward dipping slab (e.g. van Hinsbergen *et al.* 2014).

Most authors propose that between these two stages, the Algerian basin evolved in relation to a rollback process of the Tethyan slab (Alvarez *et al.* 1974; Cohen 1980; Lonergan & White 1997; Doglioni *et al.* 1999; Frizon de Lamotte *et al.* 2000; Jolivet & Faccenna 2000; Faccenna *et al.* 2001; Gelabert *et al.* 2002; Rosenbaum *et al.* 2002; Mauffret *et al.* 2004; Schettino & Turco 2006; van Hinsbergen *et al.* 2014) enhanced by slab tears to the west and to the east, in good agreement with tomographic studies (Fig. 1a; Spakman *et al.* 1993; Carminati *et al.* 1998; Piromallo & Morelli 2003; Spakman & Wortel 2004; Bezada *et al.* 2013; Palomeras *et al.* 2014; Thurner *et al.* 2014), however the timing and the geometry of the southward European forearc migration are still a matter of debate. To the west, the westward rapid slab rollback under the Alboran Sea would be responsible for the Miocene opening of the western Algerian basin (Réhault *et al.* 1984; Gueguen *et al.* 1998; Jolivet & Faccenna 2000; Vergés & Fernàndez 2012; Medaouri *et al.* 2014; van Hinsbergen *et al.* 2014). Here, the westward verging slab would still be attached to the surface lithosphere beneath the Betic and Rif belts, but would be detached under the Alboran (Palomeras *et al.* 2014; Thurner *et al.* 2014), where the lithospheric mantle might be driven into the asthenospheric mantle (Bezada *et al.* 2013; Palomeras *et al.* 2014; Thurner *et al.* 2014). Recent studies devoted to the crustal structure of the western Algerian margin and the adjacent basin have proposed that the surface expression of the slab tear in this area is a 'STEP' fault (subduction-transform edge propagator; Govers & Wortel 2005) that is edging the western Algerian basin to the south (Vergés & Fernàndez 2012; Medaouri *et al.* 2014; Badji *et al.* 2015) and follows the slab retreat parallel to the continent–ocean boundary (Medaouri *et al.* 2014; Badji *et al.* 2015).

To the east, the subduction is still active under the opening Tyrrhenian basin (e.g. Jolivet & Faccenna 2000; Rosenbaum & Lister 2004a; Rosenbaum *et al.* 2008; Gallais *et al.* 2013). The way the slab migrated from the Kabylian area to its present-day position is not clear, mainly because the evolution of the eastern Algerian basin remains poorly understood. In particular, little is known about its crustal structure, and that of its southern margin. While some studies have proposed that the deep basin has resulted from delamination of a continental lithosphere (Roure *et al.* 2012), most studies have considered the eastern basin as an oceanic domain that was formed by backarc accretion, bounded to the south by its continental margin (Alvarez *et al.* 1974; Cohen 1980; Lonergan & White 1997; Doglioni *et al.* 1999; Frizon de Lamotte *et al.* 2000; Jolivet & Faccenna 2000; Faccenna *et al.* 2001; Gelabert *et al.* 2002; Rosenbaum *et al.* 2002; Mauffret *et al.* 2004; Schettino & Turco 2006). According to these models, the eastern Algerian margin might instead be considered a rifted stretched (e.g. Gueguen *et al.* 1998; Jolivet & Faccenna 2000), or transcurrent (e.g. Mauffret *et al.* 2004; Schettino & Turco 2006), continental margin segment, with implications on the way the slab escaped to the east.

The aim of this study was to determine the crustal structure of the eastern Algerian basin and its southern margin in the Annaba region (Fig. 2a), to better constrain the kinematic models of the eastern Algerian basin and the eastward migration of the slab. This study is based on: (1) new data acquired in 2009 during the Sismique Profonde et Investigation Régionale au Nord de l'Algérie (SPIRAL) cruise, which included a 240-km-long onshore-offshore wide-angle seismic profile, deep-penetrating multichannel seismic (MCS) lines and gravimetric and magnetic data (Fig. 2a); and (2) additional available data that included multibeam bathymetry and high-resolution seismic data, industrial deep-penetrating MCS data, and complementary gravimetric and magnetic data (Fig. 2a).

2 GEOLOGICAL SETTING

2.1 Kinematic reconstruction of the eastern Algerian basin

The eastern Algerian basin forms a 150 00 km^2 basin that is bounded by the eastern Algerian margin to the south, the Sardinia Channel to the east, the Liguro-Provencal basin to the north, and the western Algerian basin to the west (Fig. 1a). Its oceanic nature is suggested by an ∼400-km-wide and ∼200-km-long set of magnetic anomalies that trend N–S to NW–SW as they diverge southward within the eastern Algerian basin (Fig. 1a, insert; Galdeano & Rossignol 1977; Schettino & Turco 2006). Indeed, these are the only clear, regularly organized, magnetic anomalies that have been identified in the western Mediterranean domain. In other parts of the basin, disorganized magnetic anomalies have been interpreted as the result of irregular and sporadic accretion processes at the back of the subduction zones, based on the atypical structure of the oceanic crust (Contrucci *et al.* 2001; Rollet *et al.* 2002). In contrast, the set of regular anomalies observed within the eastern Algerian basin suggests that a steady oceanic accretion occurred in this part of the basin. The timing and geometries proposed for the formation of this part of the basin, however, vary from one model to another, mainly because the age of these anomalies is still not known. In the simplest model, the Algerian basin opened at the back of the AlKaPeCa blocks, as it migrated to the south with an arcuate shape (Gueguen *et al.* 1998; Jolivet & Faccenna 2000; Gelabert *et al.* 2002; Rosenbaum *et al.* 2002; Rosenbaum & Lister 2004b; Michard *et al.* 2006; Schettino & Turco 2006). The set of regular anomalies was explained by an oceanic accretion stage that resulted from the coeval divergent southward displacement of the Kabylies, and the Corso–Sardinian block toward the east (Gelabert *et al.* 2002), possibly along a complex spreading system that involved transform faults and triple junctions (Schettino & Turco 2006).

Other models have proposed a two-stage oceanic opening. In these two-stage models, the south and southeast migration of the

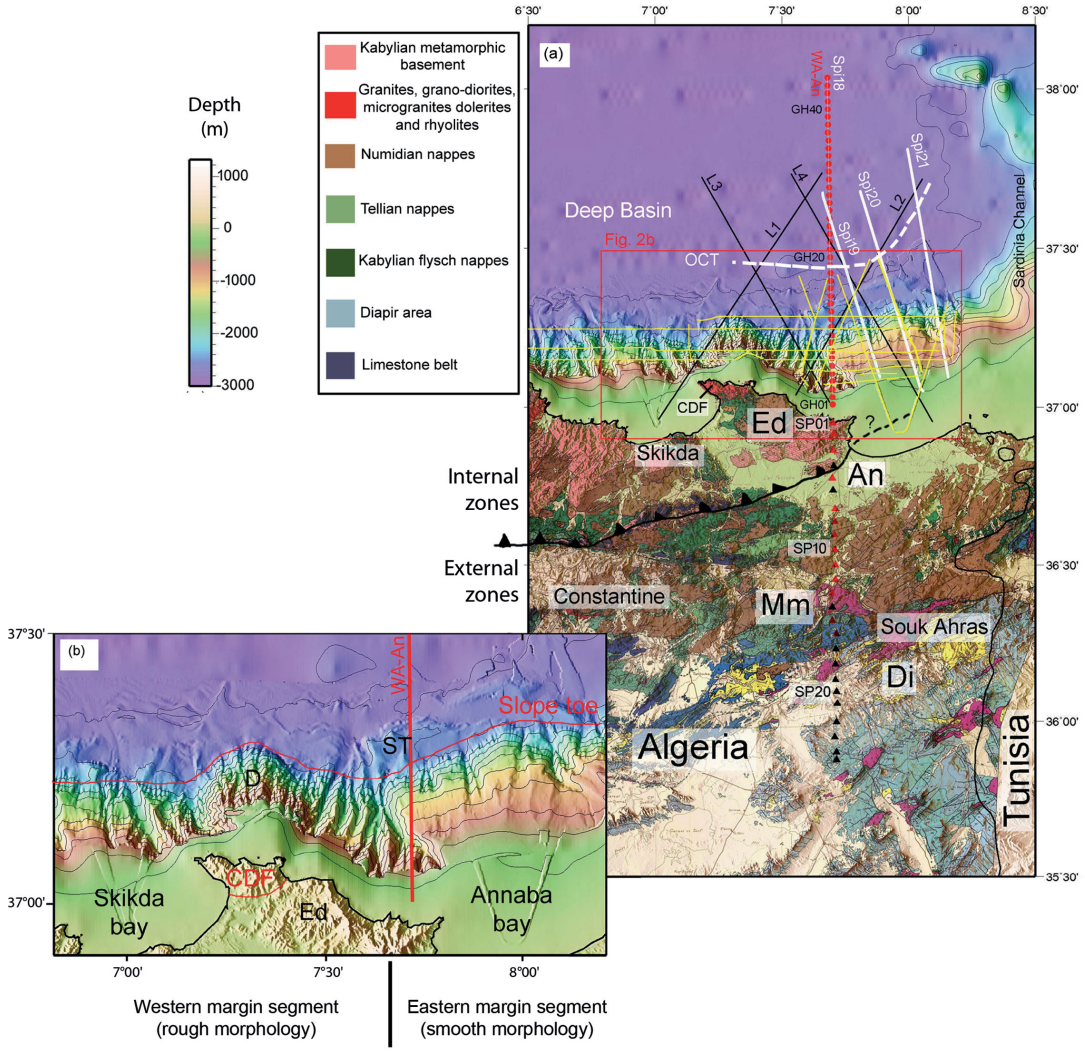

Figure 2. (a) Location of the data set used in this study, superimposed on the bathymetric map provided by Maradja2/Samra cruise (2005) (Kherroubi *et al.* 2009) and by ETOPO1 1-min global relief (www.ngdc.noaa.gov) in the offshore domain, and on the eastern Algerian geological map in the onshore domain (Vila 1978). The geological map shows the different structural units of the study area including the Internal zones (Lesser Kabylia, Fig. 1, LK) and External zones (Tell). Ed, Edough massif; CDF, Cap de Fer; An, Annaba basin; Mm, Mellègue Mountains and Di, Diapir area. Red dots, OBS position (numbered GHxx); Triangles, land station position (numbered SPxx); Red triangles, stations which recorded usable data. Black triangles: stations recorded only noise. White lines: location of the multichannel seismic lines, magnetic and gravity data acquired during SPIRAL cruise. Black lines: location of the seismic reflection, gravity and magnetic data provided by Sonatrach. Yellow lines: high-resolution seismic profiles acquired during Maradja2/Samra cruise (2005). Red frame: location of the area displayed in (b). White dotted line (OCT): ocean-continent transitional zone after this study. (b) Bathymetric map of the study area from Maradja2/Samra cruise (2005) (Kherroubi *et al.* 2009) and from ETOPO1 1-min global relief (www.ngdc.noaa.gov). CDF, cap de Fer, Ed, Edough massif.

AlKaPeCa and Corso-Sardinia blocks was followed by oceanic accretion along a NW–SE spreading centre, which led to the observed regular anomaly pattern (Cohen 1980; Mauffret *et al.* 2004). As the Corso-Sardinia block is assumed to be fixed in its present-day position from 15 to 18 Ma, this implies that an ∼400-km-wide oceanic domain opened toward the west. This might have been accommodated either by a N–S intra-oceanic subduction located at ∼5°30′E (Cohen 1980), or by the western migration of the neo-formed oceanic floor along a transform zone located north of the Algerian margin (Mauffret *et al.* 2004). In the first case, the oceanic accretion allowed the southwestward migration of the Lesser Kabylia toward the African margin after the Greater Kabylia collage (Cohen 1980). In the second case, the accretion occurred after the coeval Greater and the Lesser Kabylia collages (Mauffret *et al.* 2004). These two-stage models where accretion occurred after the main collision phase are compatible with a STEP-fault evolution of the margin following the slab tear and the eastward migration of the slab along the eastern Algerian margin, symmetrical to the evolution proposed for the western Algerian margin by Medaouri *et al.* (2014) and Badji *et al.* (2015).

2.2 Geology of the onshore domain

The north Algerian geology derives from the Tethys Ocean closure during the Algerian basin opening, and the subsequent collage of the AlKaPeCa blocks along the North African margin. This is marked by the southward thrusting of the internal zones, formed by the Palaeozoic European crystallophyllian basement of the AlKaPeCa blocks and its Mesozoic carbonated sedimentary cover, which is represented by the limestone of the 'Dorsale Kabyle' (Rivière *et al.* 1977; Bouillin 1979; Géry *et al.* 1981; Djellit 1987; Bracene 2001), over the external zones formed by the North African

margin (Fig. 2a). The North African margin is composed of parautochthonous Tellian units that include sediments from Trias to Eocene times (Fig. 2a), which lie above the African basement that outcrops more than 180 km south of the shoreline. Between the internal and external zones, the suture zone is marked by flysch units of various ages. These correspond to allochthonous clastic sediment deposited in the closed Tethyan oceanic domain, and include the Massilian and Mauritanian flysch, which have been interpreted as Cretaceous deposits (Djellit 1987), and the Numidian flysch, which has been interpreted as Oligo-Miocene deposits (Bouillin *et al.* 1970). These allochthonous flysch formations are found on the foreland, although they are also backthrusted on the internal zones (Fig. 2a; Durand-Delga 1969).

The onshore part of the study area includes the different units of this Alpine collision zone: along the shoreline, the Edough Massif (Fig. 2a, Ed) corresponds to a crystallophyllian basement that is composed of a variety of Neoproterozoic and Palaeozoic metamorphic rock (Laouar *et al.* 2002), which is locally overlain by allochthonous flysch, and has intrusions of eruptive rock (Hilly 1962). The origin of this massif has been debated for a long time. Although at first it was considered as part of the African margin (Vila 1980; Bouillin 1986; Frizon de Lamotte *et al.* 2000; Caby *et al.* 2001), recent studies indicate that it is part of the European basement that forms the eastward extension of the Lesser Kabylia, and thus is part of the internal zones (Laouar *et al.* 2002; Bruguier *et al.* 2009). South of the Edough Massif, there is a large sedimentary basin that is formed by the African Mesozoic to Cenozoic sedimentary cover, between the Mellegue Massif and the Saharan flexure, with this area characterized by intense Triassic salt diapirism [Fig. 2a, 'diapir area' (Di); Dubourdieu 1956; Rouvier 1977; Chikhi Aouimeur 1980; Pertthuisot & Rouvier 1992]. Between the diapir area and the Edough Massif, the E–W elongated, Quaternary Annaba basin extends over an area of ∼1200 km^2 (Fig. 2a, An). The Cretaceous to Oligo-Miocene flysch consists of several sheets that deformed and stacked along thrusts, to form an ∼1.5-km-thick sediment pile with a complex internal structure (Hilly 1962). The Numidian flysch is particularly well represented SE of Annaba, where its outcrops over 3500 km^2 (Fig. 2a). The accurate location of the Alpine suture is not known in the study area. It is probably located underneath the flysch cover, south of the Edough Massif, and it probably extends to the east in the offshore domain (Fig. 2a).

2.3 Geology of the offshore domain

Little is known about the deep crustal structure offshore of the Annaba region. Indeed, previous studies have essentially been based on high-resolution seismic reflection data, which resulted in detailed imaging of the recent sedimentary cover. These data show that the margin and the deep basin edge were reactivated by contraction during the Plio-Quaternary (Kherroubi *et al.* 2009), with the recent margin inversion indicated by older deep penetrating seismic profiles (Mauffret 2007). The average Moho depth, as given by gravity modelling of the European Plate, is of the order of 25 km below the margin and 15 km below the deep basin (Grad *et al.* 2009). East of the Annaba area, the Sardinian Channel is underlain by a 10-km-thick to 25-km-thick continental basement that is overlain by a 4-km-thick sedimentary cover, as shown by the wide-angle seismic data from the European Geotraverse project (Peirce & Barton 1992). The basement crops out on Galite Island (Fig. 1a), and this is interpreted as part of the internal zones (Tricart *et al.* 1994; Bouillin *et al.* 1998; Mascle *et al.* 2004; Belayouni *et al.* 2010).

3 ACQUISITION, DATA QUALITY AND PROCESSING

In the present study, new geophysical data was acquired during the SPIRAL cruise, which was conducted on the R/V Atalante (Ifremer) in September–November 2009, along the Algerian margin. During this cruise, one onshore–offshore, wide-angle seismic profile (Fig. 2a, WA-An), four MCS lines, and magnetic and gravity data were recorded along the easternmost part of the Algerian margin and the adjacent deep basin (Fig. 2a, Spi18 to Spi21). MCS Line Spi18 is coincident with the wide-angle seismic profile WA-An.

The additional available data used included: (1) bathymetry and high-resolution seismic data acquired in 2005 during the Maradja2/Samra cruises (Fig. 2a, yellow lines; Déverchère *et al.* 2005; Domzig *et al.* 2006; Kherroubi *et al.* 2009; Yelles *et al.* 2009); (2) time-migrated industry seismic lines provided by Sonatrach (Fig. 2a, lines L1 to L4) and (3) gravity and magnetic data (provided by CRAAG and Sonatrach; Fig. 2a, lines L1–L4).

3.1 Wide-angle seismic data

The complete onshore–offshore profile is 240 km in length, along which 42 ocean-bottom seismometers (OBS; Fig. 2a, red circles) and 25 land stations (Fig. 2a, red and black triangles) were deployed. The average spacing between the OBS and between the land stations was 3 and 5 km, respectively. The OBS used were MicroOBS, MicroOBS+ and OldOBS from Ifremer (Auffret *et al.* 2004). The land stations used were of the Geostar-2000, Geodevice and Kinemetrics types.

The seismic source used for the wide-angle profile was a 146-l airgun array tuned to the first peak, which was composed of eight 16-l airguns and two 9-l airguns. The airgun array generated 807 shots along the profile, every 60 s, leading to 150-m shot spacing.

The marine instrument positions were corrected for drift during their descent to the seafloor using the first-arrival direct wave. Clock drift of the internal clock of the seafloor instruments was corrected linearly. On far offsets, the signal-to-noise ratio was improved by processing the OBS and land station data, to facilitate arrival identification and interpretation. The processing sequence included: spectral deconvolution (whitening), 4–18 Hz bandpass filtering (Butterworth), and automatic gain control.

Offshore, all OBS except one (which was lost; GH14) recorded good quality data (e.g. see Figs 3 and 4). For the *P*-wave arrivals, the data showed higher signal-to-noise ratio on the vertical geophone component than on the hydrophone and horizontal geophone components, with clear arrivals identifiable up to a 65-km offset in the deep basin, and a 50-km offset at shallow water depth (Figs 3a,b, and Appendix 1). *S*-wave arrivals were also observed on the horizontal geophone of 18 OBS located within the deep basin (Fig. 5b, blue dots) for offsets that ranged between ∼15 km and ∼40 km (Fig. 4). The other OBS did not show any *S*-wave, either because the seafloor instruments were equipped with hydrophone only (Fig. 5b, black dots), or because *S*-waves did not get generated or were not detectable on the dataset due to poor signal-to-noise ratio (Fig. 5b, red dots).

For the onshore part of the profile, only the 13 stations located within an 80-km range from the shoreline recorded usable data (Fig. 2a, red triangles). The absence of useful signals from the other stations was probably related to the lack of energy at large offset and/or to complex geologic structures that affected the wave propagation, rather than to dysfunction of the instruments. The data acquired showed good signal-to-noise ratio, with identifiable

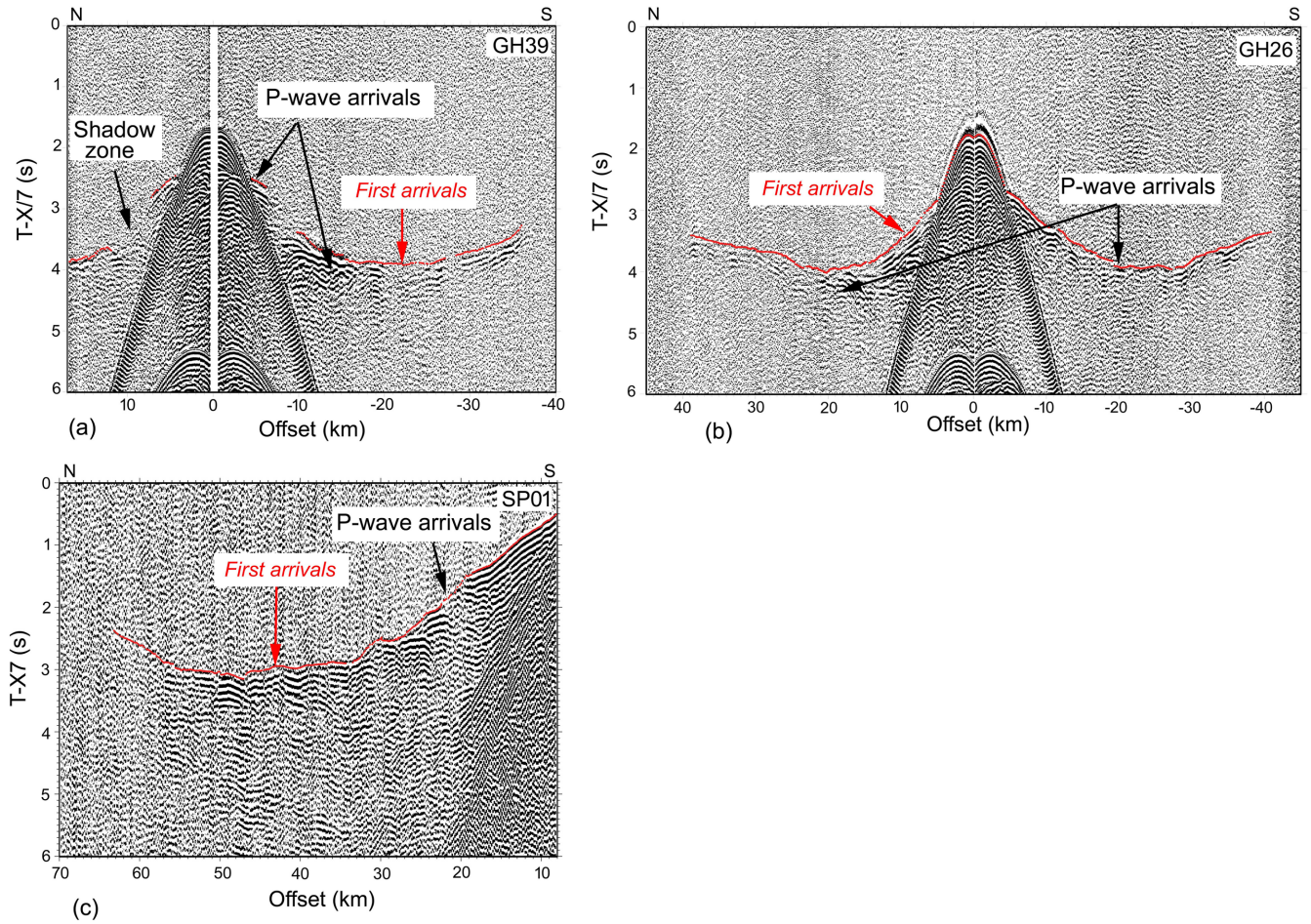

Figure 3. Examples of representative wide-angle sections recorded along WA-An profile and showing *P*-wave arrivals. (a) and (b) OBS sections (GH39 and GH26, respectively) located within the deep basin, (c) land-station section (SP01) located onshore 2 km south of the shoreline. These seismic sections correspond to the vertical component records. They were displayed after data processing including: deconvolution whitening, Butterworth filter (4–18 Hz), Automatic Gain Control (AGC), with a 7 km s^{-1} velocity reduction. Red lines: picks of the first arrivals used for first arrival tomography.

arrivals for some stations, to ∼70 km distance (Fig. 3c, Appendix 1). No *S*-waves were observed for these sections.

3.2 Multichannel seismic data

The SPIRAL MCS data (Fig. 2a, Spi18 to Spi21) were acquired using a 4.5-km-long streamer (Ifremer) composed of 360 channels with a 12.5-m interval. The seismic source was an airgun array composed of 13 airguns of various volumes tuned to the first bubble pulse, to generate low-frequency signals for deep penetration (dominant frequency, ∼25 Hz) (Avedik *et al.* 1993). The seismic source used a total volume of 3040 cubic inches (49.8 l), with an inter-shot of 20 s, which provided 50-m shot spacing. The MCS data were recorded with a 4-ms sample rate.

The processing sequence applied to the data used the Geocluster software (CGG Veritas package), and included: (1) quality control of the dataset; (2) zero-phase conversion of the single bubble wavelet; (3) common mid-point (CMP) gathering (CMP distance, 6.25 m; coverage, 45-fold); (4) reverse Q-filtering to remove the nonstationary phase components of the data, and external mute for the removal of the stretched part of the signal of the refracted waves; (5) normal moveout (NMO) velocity analyses performed every 200 CMP (1250 m), in three successive iterations; (6) spherical divergence correction based on the compensation laws (Newman 1973) and the smoothed NMO-velocity model; (7) multiple attenuation using the two complementary methods of surface-related multiple elimination based on the subtraction of a model of the multiple to the dataset (Berkhout & Verschuur 1997), and a parabolic stack radon transform based on the velocity difference between the multiples and the primaries (Bradshaw & Ng 1987); and (8) Kirchhoff pre-stack time migration. The final pre-stack time migration velocity model was obtained after five iterations of velocity picking performed on migrated CMPs every 1250 m. The processed section was plotted after application of a two-window, time-variant, Butterworth frequency filter of [3–8–20–30 Hz] and [3–8–20–30 Hz], applied from the seabed to the top of the acoustic basement, and deeper than the top of the acoustic basement, respectively (Fig. 5).

The additional multichannel seismic lines L1 to L4 of Fig. 2a were acquired and processed in 2000 by Western-Geco (Cope 2003) for Sonatrach. The seismic source consisted of a tuned first peak from a sleeve airgun array of 3000 ci (45 l) shot at a pressure of ∼2000 psi and towed at 6 m in depth (Arab *et al.* 2014; Medaouri *et al.* 2014). The shot point interval was 25 m. The receiver was a 480-channel (12.5 m each), 6000-m-long streamer towed at 8 m in depth. The processing sample interval was 4 ms for a processing record length of 10 000 ms (Arab *et al.* 2014). The processing sequence is detailed in Medaouri *et al.* (2014).

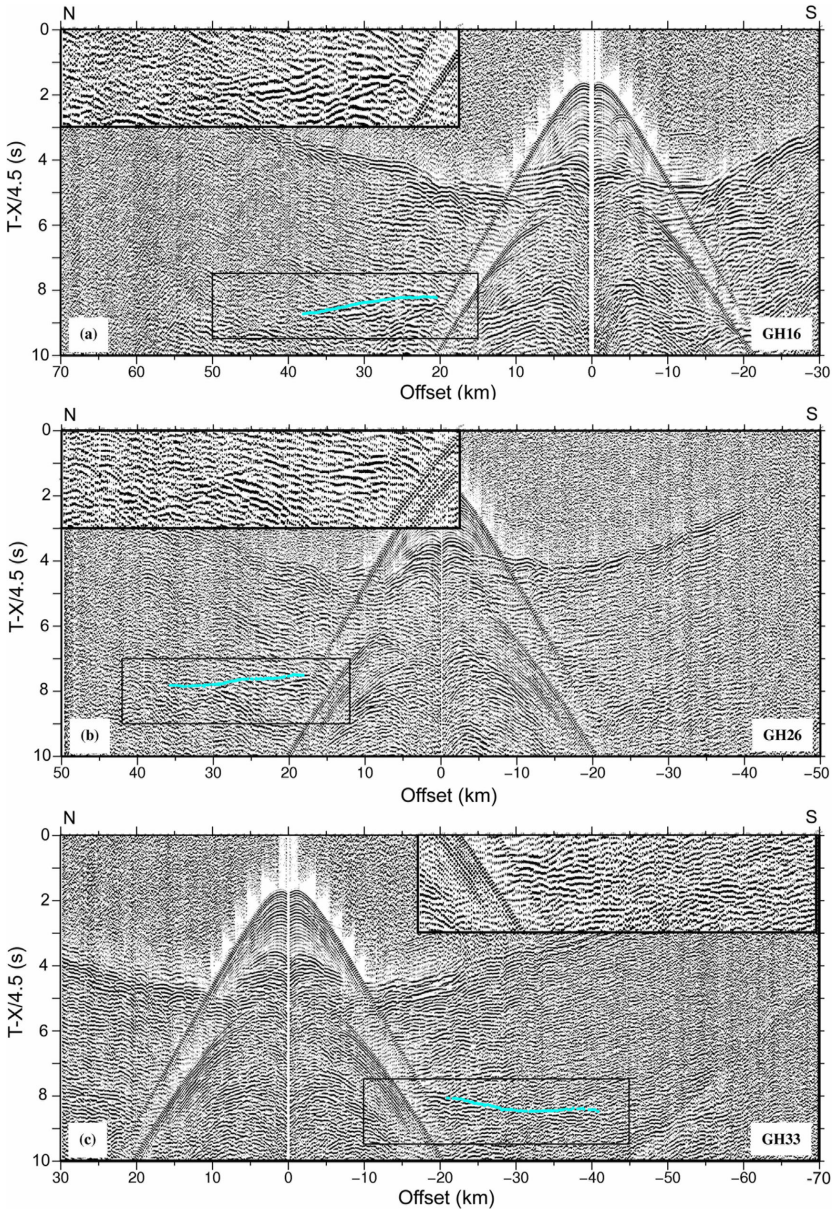

Figure 4. Examples of representative sections recorded within the deep basin along WA-An profile for (a) OBS GH16, (b) OBS GH26 and (c) OBS GH33. The black frames indicate the location of the zooms presented at the top of each seismic section. The blue dots point out the *S*-wave traveltimes used for modelling. The *S* waves come from *P*-wave conversion along subsurface interfaces. The three seismic sections correspond to the horizontal component records of the OBSs. They were displayed after data processing including: deconvolution whitening, Butterworth filter (4–18 Hz), Automatic Gain Control (AGC), with a 4.5 km s^{-1} velocity reduction.

3.3 Gravity and magnetic data

Four gravity and magnetic profiles were acquired offshore of the Annaba area during the SPIRAL cruise along the MCS lines (Fig. 2a, white lines). The gravity data were recorded with a 25-m interstation spacing, using a Lockheed Martin BGM-5 gravimeter. These data were tied to absolute gravity via a reference point located in Oran Harbor (Fig. 1a) and using a terrestrial Scintrex CG3 gravimeter. One gravity measure was recorded every 10 s, after filtering. The instrument drift was linearly corrected between ties, before and after the cruise. The Free Air and the Bouguer anomalies were calculated after Eötvös correction, with 1-mGal precision. The magnetic data were recorded at 150-m (60-s) intervals, using a SeaSPY magnetometer, which measured the total intensity of the geomagnetic field with an ∼0.2-nT precision.

The distances between the SPIRAL profiles, which were of the order of 12 km, did not provide adequate coverage for gravity and magnetic anomaly mapping, so that existing data provided by Sonatrach were also used (Fig. 2a, black lines). These existing profiles had an average length of 80 km.

4 RESULTS

4.1 Morphology

The easternmost Algerian margin is characterized by two distinct morphological domains, with the location of the wide-angle profile marking the limit between these two. West of the wide-angle

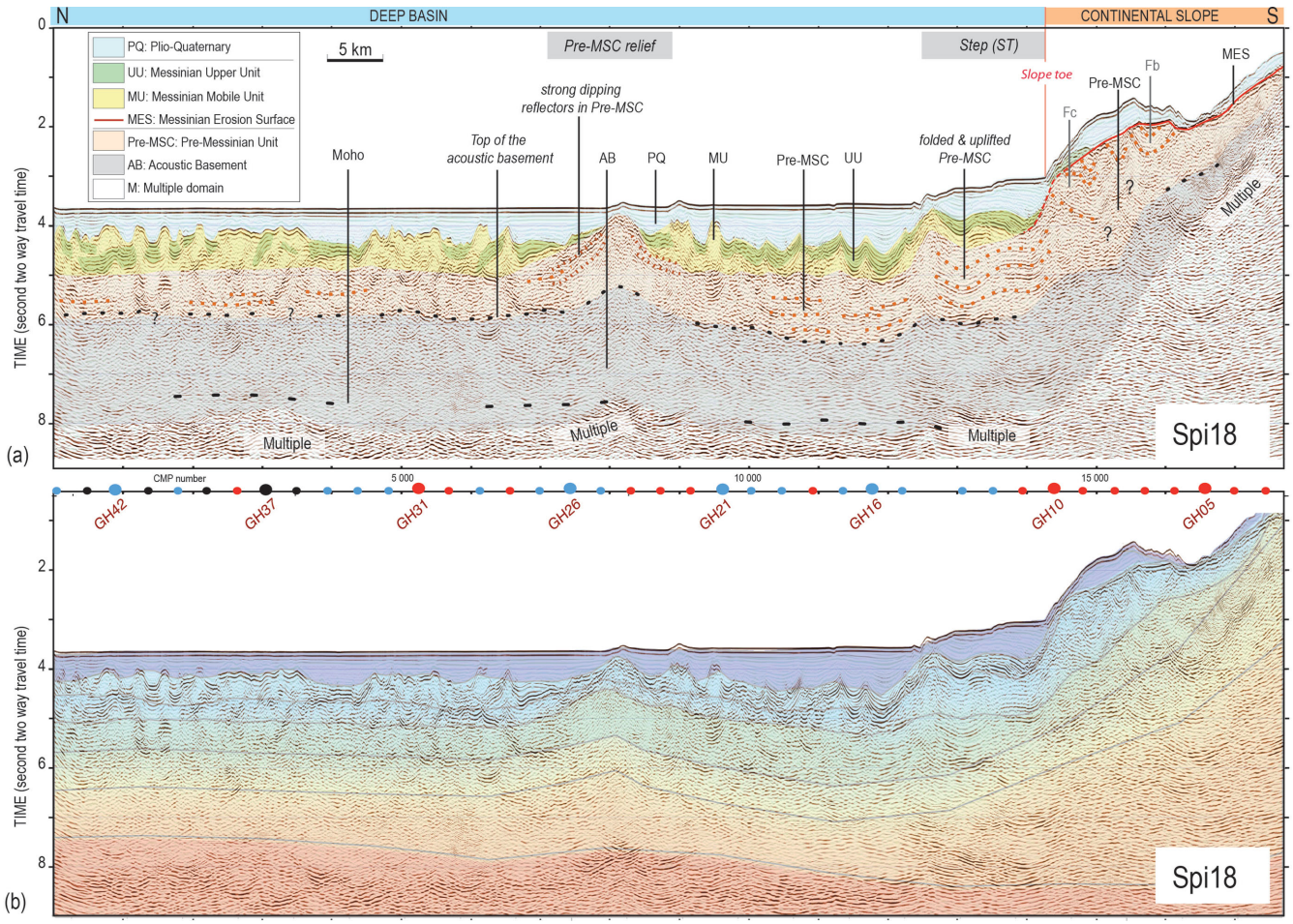

Figure 5. Time-migrated MCS profile Spi18 (coincident with the wide-angle Line WA-An; see Fig. 2a for location) with superimposition of the seismic interpretation of the line (a), and the *P*-wave velocity–depth model deduced from forward modelling of the wide-angle data converted into a two-way traveltime section (b). The dots at the top of the seismic section mark the location of the OBS (Blue dots: *S* waves observed on the horizontal geophone; Red dots: no *S* wave detected on the horizontal geophone; Black dots: No *S* wave recorded because the receivers were hydrophones only).

line (Fig. 2b, the western margin segment), the continental shelf reaches a maximum width of 15 km within the Skikda Bay, and reaches half this width west and east of the bay, offshore of Cap de Fer (Fig. 2b, CDF). The continental slope extends over 18 km and shows a regular, abrupt, 8° average slope. This sector is marked by abundant erosive gullies that generally run parallel to the slope line. Offshore of Cap de Fer, the slope has a 12-km-wide, dome-like, rounded shape (Fig. 2b, D). East of the wide-angle line (Fig. 2b, eastern margin segment), the continental shelf from Annaba Bay to the Tunisian border is wider (∼25 km) (Figs 2a and b). Here, the slope is greater, and of the order of 35 km, and it is marked by a slope break located mid-slope. The slope is gentle (4°) in its upper part, which extends over 25 km, and sharply increases at the deep slope to reach 9° on average.

The deep basin shows a smooth morphology and a uniform depth throughout the study area, with a maximum depth of ∼2800 m. The seafloor depth gradually decreases east of Line Spi21, while approaching the Sardinia Channel (Fig. 2a). Along the continental slope and between 7°35′E and 8°00′E, a ∼2500-m-deep, ∼27-km-long step overhangs the rest of the abyssal plain (Fig. 2b, ST). This step was interpreted as the result of recent margin reactivation (Kherroubi *et al.* 2009).

4.2 Multichannel seismic data interpretation

4.2.1 Architecture of the acoustic units

The seismic interpretation proposed below is based on the seismic units defined in previous studies conducted on the Algerian margin and within the adjacent deep basin. All of these studies use the Messinian units (as mobile unit [MU] and upper unit [UU]) and surfaces (as Messinian erosion surface [MES]) for chronostratigraphic markers, as they can be recognized easily in the seismic lines (Auzende 1978; Déverchère *et al.* 2005; Domzig 2006; Domzig *et al.* 2006; Mauffret 2007; Kherroubi *et al.* 2009; Yelles *et al.* 2009) and they have been well dated (5.96–5.32 Ma; Gautier *et al.* 1994; Krijgsman *et al.* 1999). We thus defined three sedimentary seismic units, as Messinian (UU-MU), pre-Messinian (Pre-MSC) and post-Messinian (Plio-Quaternary, PQ) units, using the nomenclature proposed by Lofi *et al.* (2011a,b) on the basis of a recent compilation of Mediterranean studies. It should be noted that a Messinian lower unit (LU) is observed locally within the Mediterranean Sea below a MU (Lofi *et al.* 2011a,b; Arab *et al.* 2014). However, because the Messinian LU could not be clearly identified in the low-resolution dataset of the study, it was included in the Pre-MSC unit in our interpretation of the seismic data.

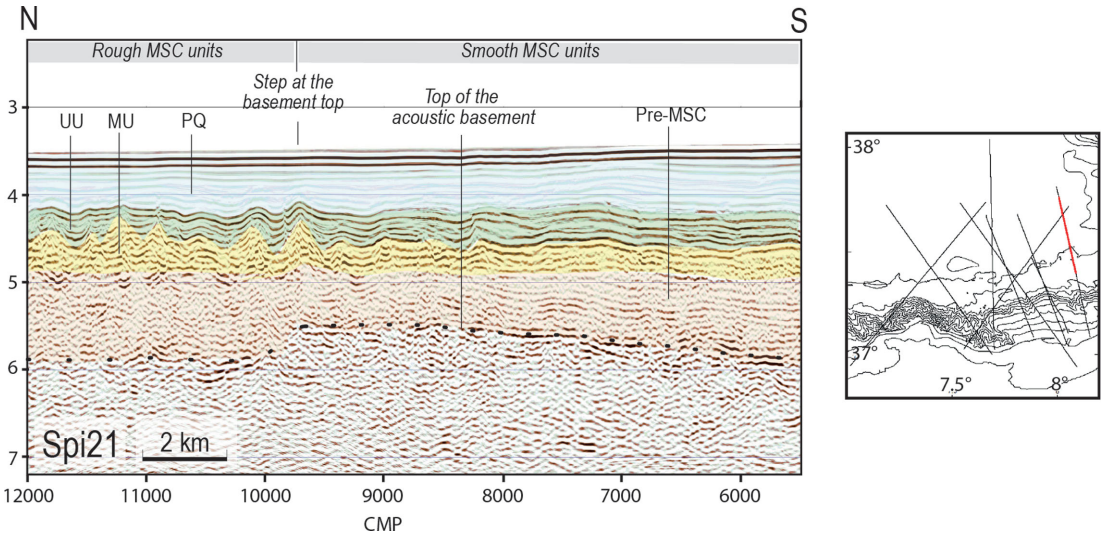

Figure 6. Time-migrated MCS Line Spi21 (see Fig. 2a for location) and seismic interpretation. PQ, Plio-Quaternary unit; UU, upper Messinian unit; MU, mobile Messinian unit; Pre-MSC, pre-Messinian unit. In the northern part of the seismic line, the reflector marking the top of the basement is weak, and lies at a constant depth of ∼5.8 stwtt, whereas it is more continuous and shallower in its southern part. This change in the top of the basement morphology corresponds to a change in the Messinian unit facies, from rough to smooth.

4.2.2 Acoustic units in the deep basin

Along the main MCS profile (Spi18), which is coincident with the wide-angle profile, the Messinian units form a clear set of reflectors within the sedimentary cover observed between 4-s and 5-s two-way travel times (stwtt) in the deep basin (Fig. 5, Spi18). These units consist of the UU and the underlying MU. The UU is ∼0.35-stwtt thick, and has a typical layered facies that shows high amplitude, and high continuity reflectors (Lofi *et al.* 2011a). Below UU, the MU forms folds and diapirs. The top of the MU is observed at ∼4.4 stwtt, which is mostly the same depth as elsewhere in the western Mediterranean (Domzig 2006; Kherroubi *et al.* 2009; Lofi *et al.* 2011a). We note a slight change in the Messinian unit facies and deformation along the seismic line. Close to the margin, the UU reflectors appear to be continuous and the salt tectonics are characterized by well-designed folds and diapirs, whereas far from the margin, numerous diapirs of smaller size interrupt the UU reflectors (Fig. 5). Here, the result is a complex structure of the Messinian unit, so that it is difficult to define the exact shape of the MU diapirs among a discontinuous UU unit. These Messinian units (UU, MU) pinch out along the margin toe at 2.6 stwtt and 4.0 stwtt, respectively (Fig. 5).

Above the Messinian units, the PQ unit is characterized by high continuity, low amplitude reflectors. The PQ unit thickens from the central part of the deep basin to the margin toe, from ∼0.3 stwtt to ∼1 stwtt.

Below the UU and MU units, the Pre-MSC unit is characterized by sub-horizontal stratification, especially at the southern edge of the basin below the bathymetric step (Fig. 5, ST). The Pre-MSC unit shows a relatively constant thickness in the central part of the deep basin (∼1–1.2 stwtt), to the northern edge of the bathymetric step. Here, the thickness of the Pre-MSC unit sharply increases, to reach ∼1.7 stwtt below the bathymetric step.

Far from the margin, the top of the acoustic basement is marked by an irregular, discontinuous reflector at ∼5.8 stwtt depth. As this approaches the margin, it shows enhanced continuity and it deepens to 6.5 stwtt (Fig. 5). At the basin edge, the Pre-MSC and MSC units are folded and uplifted below the bathymetric step. The vertical throw of the seismic markers along the northern step edge, which was of the order of ∼0.6 stwtt, has been explained by Plio-Quaternary contractive deformation of the margin (Kherroubi *et al.* 2009).

Similar facies and distribution of the shallowest acoustic units are observed throughout the deep basin of the study area. In particular, the discontinuous basement top shows a uniform depth of ∼5.8 stwtt through the deep basin, ∼15 km from the slope toe and beyond. In the ∼15-km-wide area that bounds the margin, the top of the basement has enhanced continuity and smoother morphology as it deepens, to reach 6.5 stwtt to 6.9 stwtt, as the Pre-MSC unit is thicker in this area. An exception is the easternmost part of the area, where the basement top lies at ∼5.5 stwtt over a 35-km distance from the slope toe (Fig. 6). Here, it is thus shallower than elsewhere in the vicinity of the margin. All along the eastern part of the Algerian margin, the changes in the basement top geometry and facies toward the margin coincide with the lateral change in the Messinian unit acoustic facies described above for Line Spi18.

At CMP number ∼8000 along Line Spi18, an ∼15-km-wide relief is formed by the top of the pre-Messinian unit (Fig. 5). The Messinian and post-Messinian units bevel on the relief sides, whereas the pre-Messinian reflectors dip gently toward the relief edges. This relief is also observed along Line Spi19 (see Fig. 2a for location), at its junction within Line Spi18.

4.2.3 Acoustic units on the continental margin

Along Line Spi18, below the continental slope and the continental shelf, the Messinian event is characterized by a MES that truncates the underlying reflectors (Fig. 5). Above the MES, the PQ unit has a thickness of between 0.1 stwtt and 0.5 stwtt. Under the MES, the upper part of the Pre-MSC unit is characterized by sets of dipping reflectors with opposite dip (Fig. 5). To go further into the seismic interpretation of the seismic units along the margin, we used the high-resolution seismic lines available in the study area, which show different images between the eastern and western segments of the study area.

Along the eastern segment of the study area, which is marked by a smooth morphology (Fig. 2b), the high-resolution seismic reflection

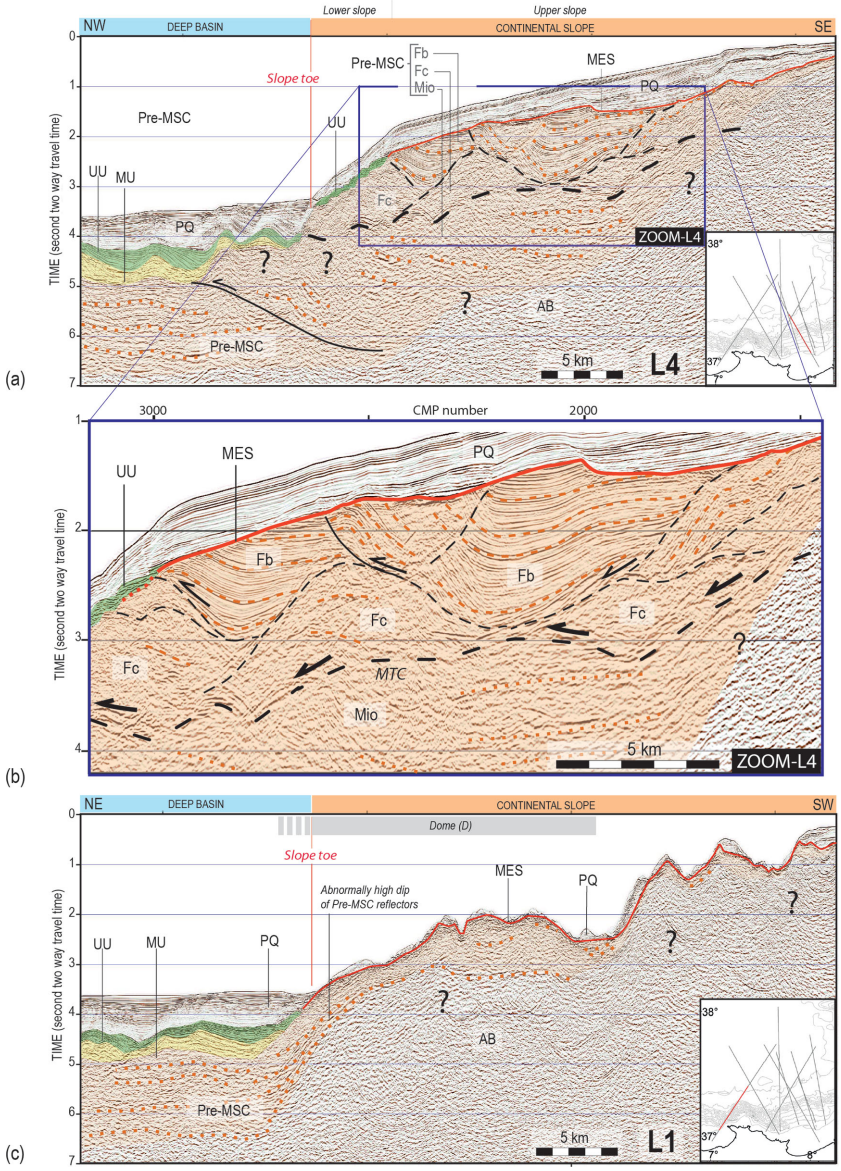

Figure 7. Seismic reflection lines and seismic interpretation illustrating the margin structure east of the wide-angle Line WA-An /Spi18 (a, b), and west of these (c). (a) Time-migrated MCS profile L4 (see Fig. 2a for location) provided by Sonatrach and its zoom of this line on the margin seismic image (b). The pre-Messinian units Fb (bedded) and Fc (chaotic) form subunits below the Messinian Erosion Surface (MES). Each subunit shows its own reflectivity and deformation patterns. The subunits limits are usually sharp and marked by clear unconformities. Fb-Fc subunits lie in unconformity over a deeper subunit Mio, characterized by low-frequency reflectors that appear less deformed than Fb-Fc reflectors. (c) Time-migrated MCS profile L1 (see Fig. 2a for location) provided by Sonatrach. West of Line WA-An/Spi18, the PQ unit is thin, and only a few reflectors are locally observed just below the PQ unit. These rare reflectors show poor lateral continuity and chaotic organization, except at the deep margin, where Pre-MSC reflectors are clearly identified over a thickness of few hundreds of milliseconds of two-way traveltime, with an unusually high dip compared to the area located east of the wide-angle Line WA-An.

lines show that the Pre-MSC unit can be split into three units: Fb, Fc, and Mio (Figs 7a and b). The Mio forms the deepest unit at the top of the acoustic basement and is overlain in unconformity by Fb and Fc, which differ from each other according to their acoustic facies. The seismic unit Fb is characterized by clear sub-parallel reflectors, whereas Fc is devoid of reflectors, or shows a chaotic pattern (Fig. 7b). The Fb and Fc units can be divided into sub-units that show lateral extensions of ∼5 km to ∼12 km. Each Fb and Fc sub-unit is characterized by its own deformation and reflectivity patterns, and the contact between the sub-units is sharp and is usually marked by clear unconformities (Fig. 7b). Locally, lateral changes in reflectivity inside some of the sub-units accompany increases in the reflector dip, which suggests that a complex internal organization prevents seismic imaging of the sub-unit reflectors (see for example Fig. 7b, for CMP numbers ∼1500 to 2000, or 2200 to 2600). The density of the available seismic lines is not sufficient to define the three-dimensional (3D) accurate spatial organization of the Fb and Fc sub-units. It is however clear that they are folded in the lines shot both parallel and perpendicular to the margin, and that the sharp contact between the folded sub-units is tectonic rather than erosive (Figs 7a and b). As the numerous folds imply a contractive tectonic environment, these contacts are interpreted as thrusts, which lead to the stacking of the subunits over thicknesses that locally reach ∼1.4 stwtt (Fig. 7a; i.e. ∼2800 m, according to the velocity–depth model). The seismic lines show that the Fb and Fc subunits are observed below the slope and up to the shelf break, which is located ∼20 km

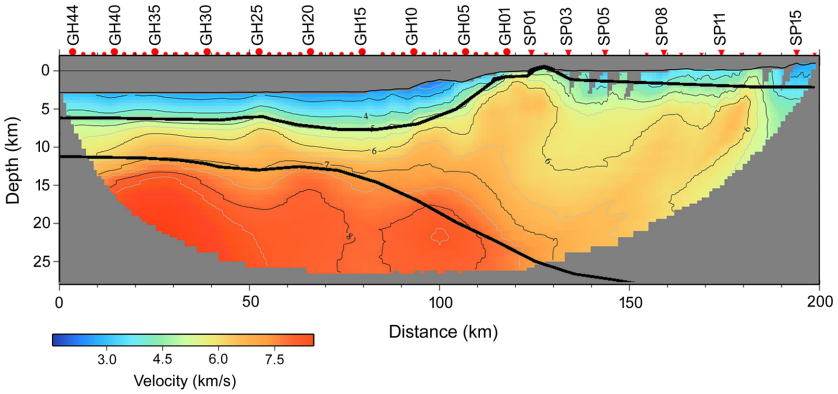

Figure 8. *P*-wave velocity–depth model deduced from seismic tomography inversion of the traveltime of the first arrivals. Isovelocity contours are displayed every 0.5 km s^{-1}. Black lines: layer boundaries taken from the forward model; Red dots: OBS locations; Red inverted triangles: land station locations.

from the shoreline (Fig. 7a). This suggests that they probably extend below the continental shelf, although at such a shallow depth, the strong multiple prevents their imaging.

Below Fb-Fc, Mio is characterized by low-frequency, low-dipping reflectors. These reflectors are characterized by a deformation pattern that differs from that observed in Fb-Fc. The Fb-Fc/Mio boundary is marked by a high-amplitude, irregularly shaped and discontinuous reflector that gently dips toward the deep basin (Figs 7a and b). Across this boundary, the clear unconformity and the change in the deformation style between Fb-Fc and Mio strongly suggest that it corresponds to a major tectonic contact that allows the emplacement of Fb-Fc sub-units above Mio.

Along the western segment of the study area marked by rough morphology (Fig. 2b), the seismic image is very different from that of the eastern segment. The MES shows an irregular topography (Fig. 7c). The PQ unit is thinner than in the eastern segment, with a thickness between 0 stwtt and 0.3 stwtt that shows local thickening up to ∼0.4 stwtt. In this area, the maximum penetration below the Messinian surface is of the order of ∼1.7 stwtt, and is thus much lower than in the eastern zone. Only a few, low-frequency reflectors are observed locally just below the PQ unit. These rare reflectors show poor lateral continuity, except at the deep margin, where Pre-MSC reflectors are clearly identified over a thickness of a few hundreds of milliseconds of two-way times (Fig. 7c). Here, the Pre-MSC reflectors show abnormally high dip, compared to elsewhere in the study area.

4.3 Wide-angle seismic data modelling

4.3.1 First arrival seismic tomography

The travel-times of all first arrivals were picked (Fig. 3) and modelled using the Tomo2D tomographic inversion code, to calculate the velocity field along the onshore-offshore wide-angle seismic profile (Korenaga *et al.* 2000). A weight was assigned to the picks according to the quality of the seismic data. This quality depends on the signal-to-noise ratio, and the signal impulsiveness and lateral continuity on several consecutive shots. Four quality levels were defined for the first arrival picks, based on the picking uncertainty. This picking uncertainty was estimated as the time difference between a given pick and the averaged line crossing the 10 neighboring picks. This varied from 0.016 s (twice the sampling interval) for the clearest arrivals observed at the small offset and/or with high amplitude, to 0.1 s for noisy and less-impulsive arrivals that showed low lateral coherence at large offsets. On some OBS, multiple arrivals were clearer than primary arrivals for offsets greater than 70 km. In this case, the multiple travel-times were picked and the time differences between the multiples and the primaries were subtracted for the modelling. For these picks, the uncertainty was estimated to be 0.13 s. Altogether, more than 14 000 picks were used for the modelling, including ∼38 per cent of excellent quality (uncertainty, from 0.016 to 0.035 s), ∼49 per cent of medium uncertainty (from 0.07 to 0.1 s), and 13 per cent with an uncertainty of 0.13 s.

We performed the inversion for the testing of more than 20 different initial models, with different combinations of input parameters (e.g. smoothing, damping, correlation length). The final model was selected based on the lowest root mean square (RMS) error that led to a geologically plausible structure while avoiding small artefacts that might have resulted in lower RMS, without being supported by the data. The final velocity–depth model (Fig. 8) has a RMS of 0.12.

In the deep basin, the iso-velocity lines of the velocity model are broadly horizontal (Fig. 8), with a velocity gradient greater than 0.5 km s^{-2}, and velocities between 1.6 km s^{-1} and 5.0 km s^{-1} from the seafloor down to ∼7.0 km in depth. Deeper, between 7.0 km and 12.5 km in depth, the crustal basement velocities range between 5.0 km s^{-1} and 7.0 km s^{-1}, as the velocity gradient decreases to 0.2 km s^{-2} to 0.4 km s^{-2}. A ∼20-km-long anomaly can be observed at ∼50 km along the velocity model, where the isovelocity contours representative for sedimentary layers (1.6 km s^{-1} to 3.0 km s^{-1}) dome up, and those for basement velocities between 6 km s^{-1} and 7.5 km s^{-1} deepen, thereby indicating a local thickening of the crust (Fig. 8). Below the continental slope, the shallow part of the model characterized by sedimentary velocities gradually thins toward the continent, whereas the 7 km s^{-1} isovelocity contour deepens from 12 km to 25 km, which indicates a southward gradual thickening of the crust. In the basement, the velocity gradient of 0.1 km s^{-2} to 0.2 km s^{-2} is lower than that observed for the crust of the deep basin.

This tomographic model shows the main structures of the velocity-depth distribution, but fails to image details such as velocity contrasts along interfaces, velocity inversions, or highly detailed velocity gradients in the subsurface layers, as only first arrivals are used and the grid size was 0.5 km × 0.5 km. To better constrain these parameters, forward-type modelling was performed using a combination of information taken from the wide-angle data and from the coincident reflection MCS profile Spi18.

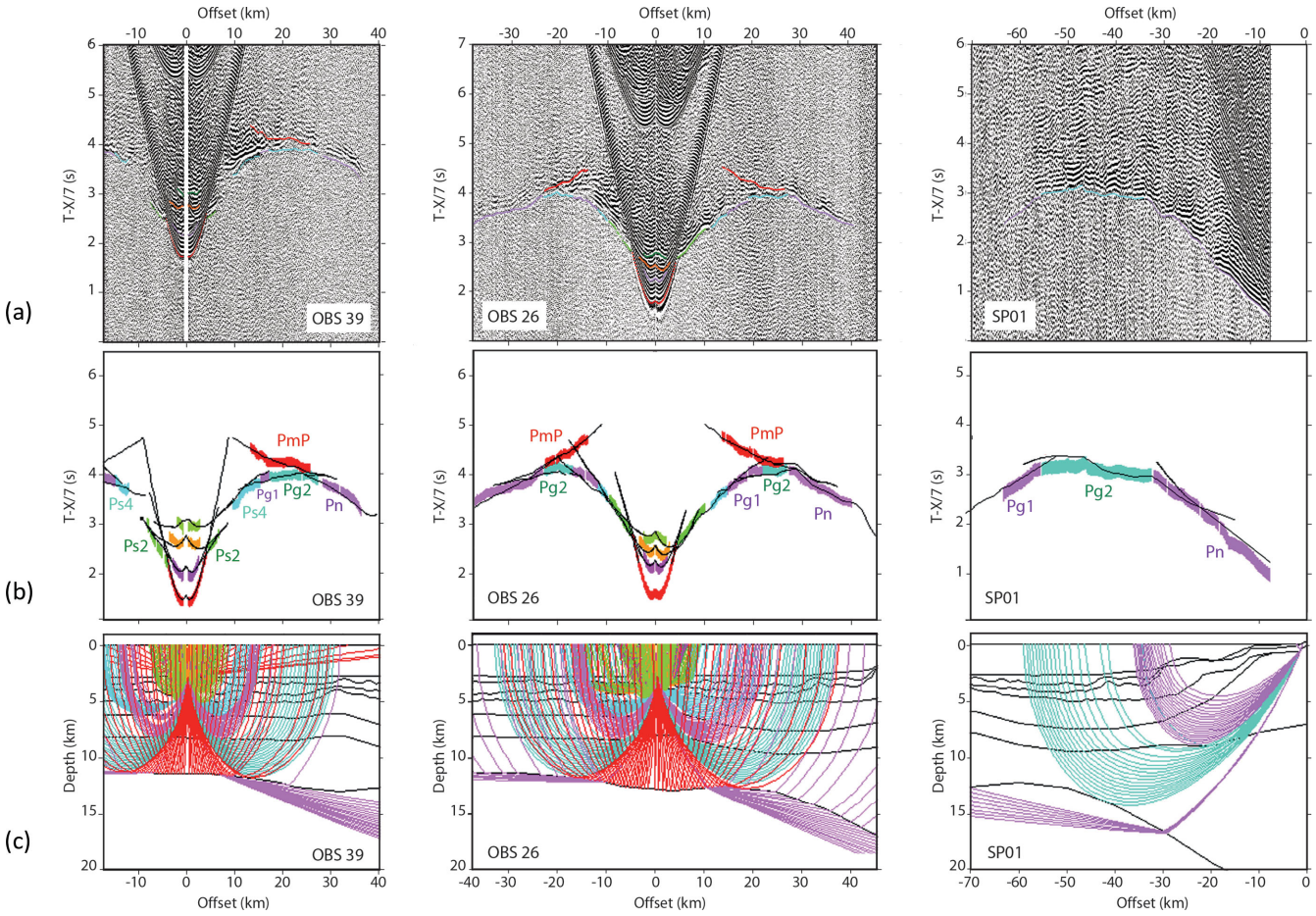

Figure 9. Forward modelling of the refracted and reflected arrivals performed for OBS GH39 (left-hand panel), OBS GH26 (centre panel) and the land station SP01 (right-hand panel). (a) Picks of the first and second arrivals superimposed on the data, (b) observed travel times plotted with the picking uncertainty and calculated travel times produced by ray tracing and (c) ray tracing through the *P*-wave velocity–depth model.

4.3.2 Forward modelling of P-wave travel-times

The forward modelling consisted of 2D ray tracing within a 2D velocity-depth model to fit the observed travel-times of both the refracted and reflected arrivals observed in the dataset (Zelt & Smith 1992) (Fig. 9). The modelling was performed on the set of first arrival picks that were previously used for the tomographic inversion, complemented by a set of secondary arrivals picked from refracted and reflected *P*-waves (Fig. 9a and Appendix 1), considering an uncertainty between 0.03 and 0.13 s. The geometry of the sedimentary layer boundaries was given by the interfaces picked along the coincident MCS Line Spi18 (Fig. 5a). The depth of the layers was then adjusted using velocity information determined from the wide-angle seismic data, from top to bottom of the model, to reduce the misfit between the observed and calculated travel-times (Figs 9b and c).

The quality of the velocity-depth model is evaluated by considering the fit between the predicted and observed travel-times, which was evaluated by the RMS error and the chi-square (χ^2) parameter. The χ^2 is defined as the RMS travel-time misfit between the calculated and observed arrivals normalized to the picking error. The RMS travel-time misfit obtained was 0.114, with a χ^2 of 1.799, for a total number of 22 289 picks correctly reproduced by modelling (Table 1). These modelled picks correspond to more than 87 per cent of the 25541 arrivals picked along the seismic sections, including the refracted and reflected waves. Given the large number of modelled picks for the Pg (8360), Pn (2815) and PmP (2357) taken into account for modelling (Table 1), even the deep structure was constrained with confidence.

Table 1. Residual traveltimes and χ^2 errors for all of the phases picked along the Annaba wide-angle profile.

Phase	Number of modelled picks	Rms error (s)	χ^2 error
Water	1865	0.035	0.245
Ps2	1207	0.077	1.202
Ps3	1905	0.123	3.065
PsP1	958	0.060	0.739
PsP2	1406	0.067	0.919
PgP1	1416	0.072	1.504
Pg1	2391	0.107	1.550
Pg2	5969	0.153	2.877
Pn	2815	0.118	1.698
PmP	2357	0.111	1.490
All phases	22289	0.114	1.799

Two-point ray tracing between source and receivers shows well-resolved and unconstrained parts of the velocity model (Fig. 10). The ray coverage was generally very good, due to the good quality of the data and to the close shot and receiver spacing. In the marine part of the model, the superficial, intermediary and deep layers were well sampled by reflected and turning rays. For the continental part, the superficial and intermediary layers were less well sampled

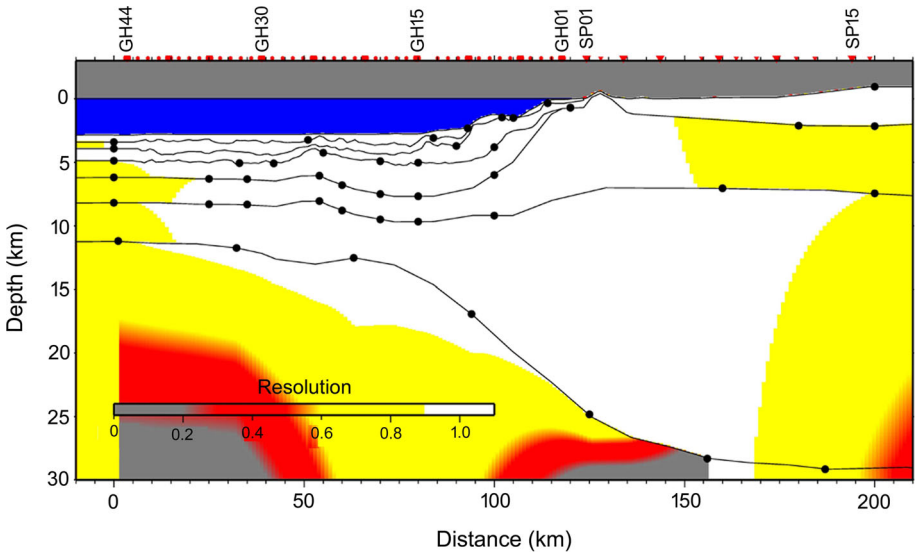

Figure 10. Resolution parameter for all velocity nodes (blacks dots) of the velocity–depth model. The white and yellow areas can be considered well resolved. A value above 0.5 is considered acceptable (Zelt 1999). The blue colour corresponds to the sea water layer.

southward towards the end of the line. This was because the shots were fired only in the marine part, which meant that the model was not reversed from 115-km to the end of the profile. In this region, the velocity–depth model was thus less constrained.

The resolution parameter was defined by the number of rays that passed along a given velocity node, and therefore it depended on the node spacing (Zelt & Smith 1992). Layers defined by a large number of velocity nodes need numerous rays that pass through each node, to be well constrained, while layers with smaller numbers of nodes can be well constrained by just a few rays that pass through the layer. Nodes with values greater than 0.5 are considered to be well resolved (Fig. 10, white and yellow areas). Most parts of the model have good resolution (values >0.7), which indicates that each velocity node is well constrained (Fig. 10). The resolution decreases to 0.5 for depths greater than 15 km offshore, because the Pn was observed only on a few OBS sections. The onshore part of the model shows a resolution of ∼0.5, due to the absence of reverse shots in this region. Care was taken to include the fewest possible velocity nodes in this region.

The 2D velocity depth model resulting from forward travel-times and amplitude modelling consists of 8 layers (Fig. 11). The water layer was modelled with a velocity of 1.54 km s^{-1}. This relatively high velocity is consistent with values reported in the literature for the Mediterranean Sea (Klingelhoefer *et al.* 2008; Gailler *et al.* 2009; Leprêtre *et al.* 2013; Mihoubi *et al.* 2014). It can be explained by the high salinity of the Mediterranean basin seawater.

The structure of the eastern Algerian margin and the adjacent deep basin offshore of Annaba was modelled according to the six units (Fig. 11) that correspond to the seismic units defined on the MCS Line Spi18 (Fig. 5), and also to the acoustic basement and the Mohorovicic discontinuity (Moho). From top to bottom, these units are:

– The PQ layer, which is modelled using velocities from 1.9 km s^{-1} to 2.2 km s^{-1}, and thicknesses from ∼400 m to ∼1000 m.

– The Messinian layer UU-MU that has velocities from 3.4 km s^{-1} to 3.8 to 4.0 km s^{-1}, and a total thickness of from 500 m to 1500 m. The two Messinian units UU and MU are modelled by a single layer, as a subdivision into two layers is not required to successfully model the wide-angle seismic data, and the modelling was undertaken using the minimum structure approach. The complex shape of the top the Messinian units observed on the MCS line is slightly smoothed in the velocity model, to avoid instabilities of the modelling code.

– The pre-Messinian sedimentary units, Pre-MSC, modelled by two velocity layers: in the deep basin, the shallowest Pre-MSC1 unit has velocities from 3.0 km s^{-1} to 4.0 km s^{-1}, and the deepest Pre-MSC2 unit has velocities from 4.0 km s^{-1} to 4.8 km s^{-1}. The Pre-MSC1 unit is characterized by velocities lower than the velocities defined for the Messinian layer, and it allows the modelling of the shadow zone observed between arrivals Ps2 and Ps3 observed on some OBS records within the deep basin (Fig. 9 and Appendix 1). The Pre-MSC2 unit allows modelling of a refracted arrival Ps3 that is clearly observed in the data (Fig. 9), and that shows velocities greater than those defined for the Messinian layer. The absence of discontinuity within the Pre-MSC unit in the MCS lines (Fig. 5), and the absence of a velocity step between the Pre-MSC1 and Pre-MSC2 units within the velocity model, both suggest that this limit does not correspond to a vertical change within the sedimentary cover. Indeed, the limit between these two units marks the value of the velocity that becomes greater than the velocity within the Messinian layer, which allows the re-emergence of refracted waves.

At the continental margin, the shallowest pre-Messinian layer, the Pre-MSC1 unit, has velocities from 3.0 km s^{-1} to 4.0 km s^{-1} (Fig. 11). It is 3 km thick at the deep margin, and thins rapidly upslope. The Pre-MSC2 gradually thins below the margin, while the velocities increase from sedimentary to crustal velocities (4.0–4.8 km s^{-1} to 5.1–5.2 km s^{-1}) between 100-km and 117-km along the velocity–depth model. As the velocity–depth model is poorly constrained by the *P*-wave travel-times in the shallow southern on-land part (Figs 10 and 11), indirect constraints provided by gravimetric studies (Boubaya 2006) and by geological observations were used to build this part of the initial velocity–depth model. On land, the wide-angle line crosses the diapir area, which corresponds to the thick sedimentary cover of the African basement (Fig. 2a). Its thickness is not known accurately, although gravity modelling indicates a thickness of ∼4 km for the sedimentary layer in this area (Boubaya 2006), while a gravimetric study conducted in western

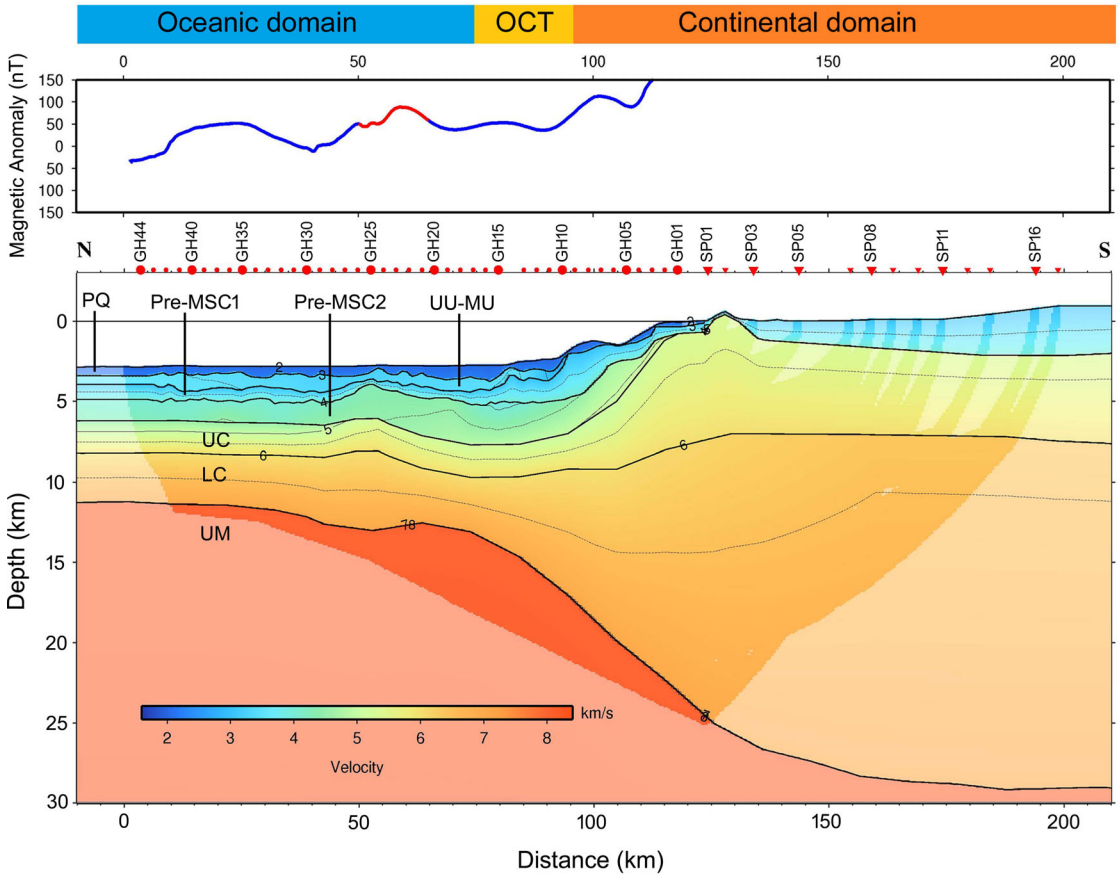

Figure 11. Results of forward *P*-wave velocity modelling along the Annaba profile WA-An. Upper panel: magnetic anomaly acquired during SPIRAL cruise reduced to pole. Lower panel: *P*-wave velocity–depth model deduced from forward modelling. Red circles: OBS location; Red inverted triangles: location of the land stations used in the modelling. Isovelocity contours are displayed every 0.5 km s^{-1}. Parts of the model that are unconstrained by ray-tracing are shaded. PQ, plio-quaternary; UU-MU, upper unit and mobile Messinian unit; Pre-MSC1, pre-Messinian layer 1; Pre-MSC2; pre-Messinian layer 2; UC, upper crust; LC, lower crust; UM, upper mantle.

Tunisia indicated that the depth of the Paleozoic sediments might exceed 5 km (Jallouli *et al.* 2005). However, it appears from forward modelling that thicknesses of the order of 4 km to 5 km did not allow correct modelling of the observed travel-times, and the best results were obtained for a 2-km-thick to 3-km-thick layer with an average velocity of 3.5 km s^{-1} (Fig. 11). It should be noted that the terrestrial part of the model is not covered by the reverse shots, and thus precise modelling of the reflectors at this place was not possible.

Below the sedimentary units, two layers with crustal velocities that correspond to the acoustic basement were identified in the MCS data. The shallowest layer that corresponds to the upper crust (UC) was characterized by velocities from 4.8 km s^{-1} to 6.0 km s^{-1}. The deeper layer that corresponds to the lower crust (LC) was defined by velocities from 6.0 km s^{-1} to 7.1 km s^{-1}. The whole crust was ∼5.5 km thick within the deep basin. However, between 40 km and 65 km along the forward velocity–depth model, a 2 km over-thickening of the basement layers can be observed (Fig. 11), which was also imaged in the tomographic model (Fig. 8). This crustal over-thickening was located below the bump formed by the Pre-MSC unit described in the MCS Line Spi18 (Fig. 5). Below the continental slope, the crustal layers showed a sharp increase in thickness from ∼7 km at the basin edge to more than 20 km at the shoreline. Here, the uppermost crustal layer reaches the surface. A similar velocity increase at shallow depth was also observed in the tomographic model (Fig. 8), which confirms its existence.

The deepest layer of the model (the upper mantle; UM) was characterized by velocities of the order of 8 km s^{-1}. The depth of the Moho was ∼12 km beneath the deep basin, and this gradually deepened below the margin, to reach ∼25 km at the shoreline.

4.3.3 *S-wave travel-time modelling*

A total of 1574 *S*-waves arrivals were picked in the deep basin (Fig. 4 and Appendix 2). These *S*-waves, which cannot be produced by the seismic source triggered in the water layer, result from a conversion of *P*- to *S*-waves at subsurface interfaces.

The modelling of the *S*-wave travel-times was performed by ray tracing, to determine the interface along which the conversion from *P*-waves to *S*-waves occurs, the layers in which the *S*-waves propagate, and the *S*-wave velocity and the related value of the Poisson's ratio (σ) in these layers, computed according to the relation:

$$\sigma = \frac{V_P^2 - 2V_s^2}{2(V_P^2 - V_s^2)}$$

In a first step, the *S*-wave velocities and the Poisson's ratio values were assumed for the different layers of the final *P*-wave velocity–depth model presented in Fig. 11, based on a compilation of values given in the literature for the oceanic crust and the underlying upper mantle (Christensen 1978; Spudish & Orcutt 1980; Purdy 1983; Karson *et al.* 1984; Price & Morgan 2000). Ray tracing in this velocity–depth model was then performed (Fig. 12), and

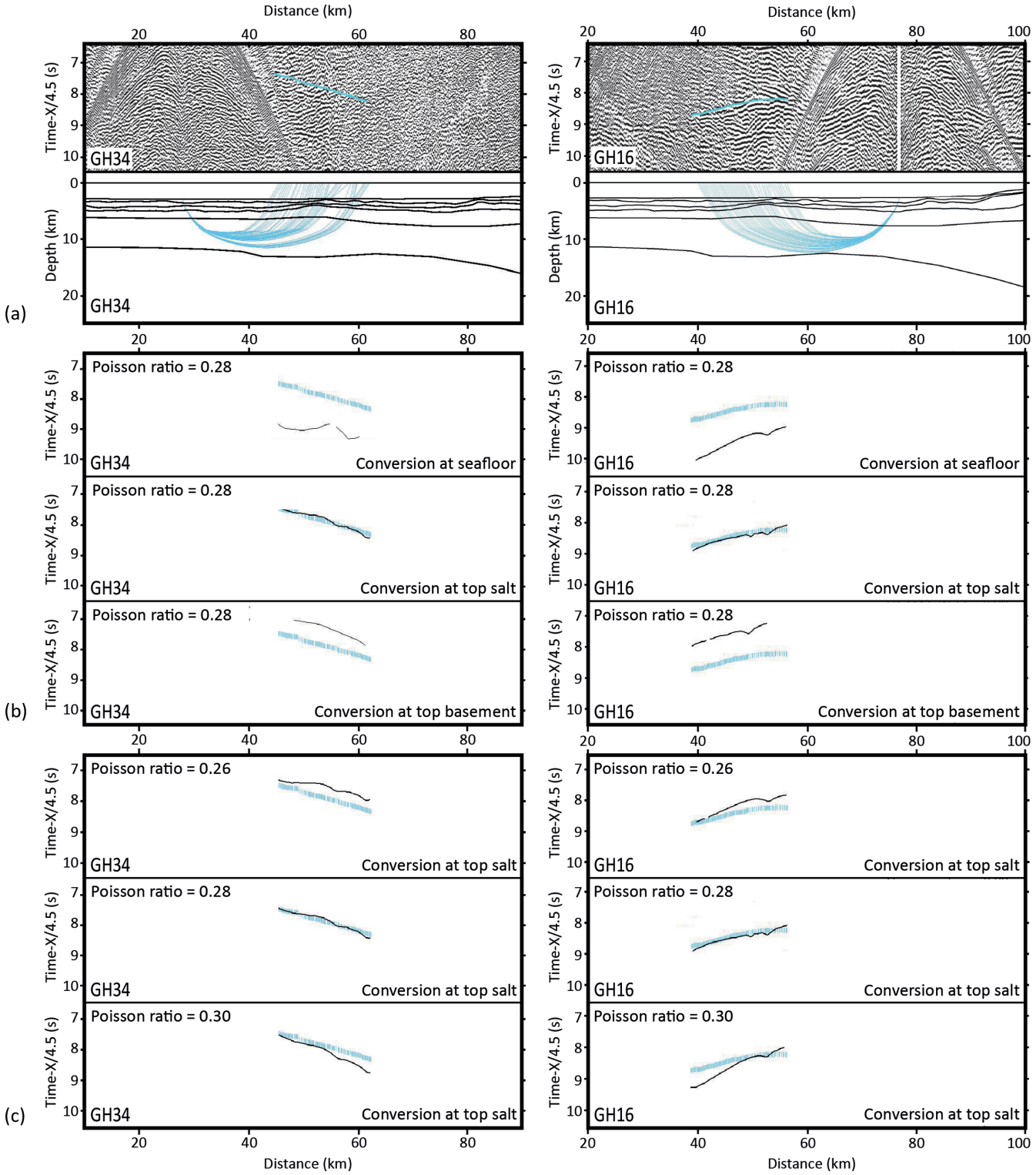

Figure 12. Examples of *S*-wave traveltime modelling by ray tracing shown for OBS GH34 (left-hand panel) and GH16 (right-hand panel) (see location of the OBSs in Fig. 5b). (a) Top panel: picks of phase PSg2 superimposed on a zoom of the seismic section. Bottom panel: example of ray tracing in the lower crust, using a Poisson's ratio of 0.28 and a *P*- to *S*-wave conversion at the top of the salt layer. (b) Ray tracing performed to test the conversion interface along which *P* waves convert to the *S* waves picked in the data, considering a Poisson's ratio of 0.28 in the LC. From top to bottom, the three panels show the observed travel-times (blue picks) and the calculated traveltimes (black line) for *P*- to *S*-wave conversion occurring at the seafloor, at the top of the salt layer, and at the top of the basement. (c) Ray tracing performed to test the Poisson's ratio in layer LC. From top to bottom, the three panels show the observed traveltimes (blue picks) and the calculated traveltimes (black line) for a Poisson's ratio in the LC of 0.26, 0.28 and 0.30, and *P*- to *S*-wave conversion occurring at the top of the salt layer.

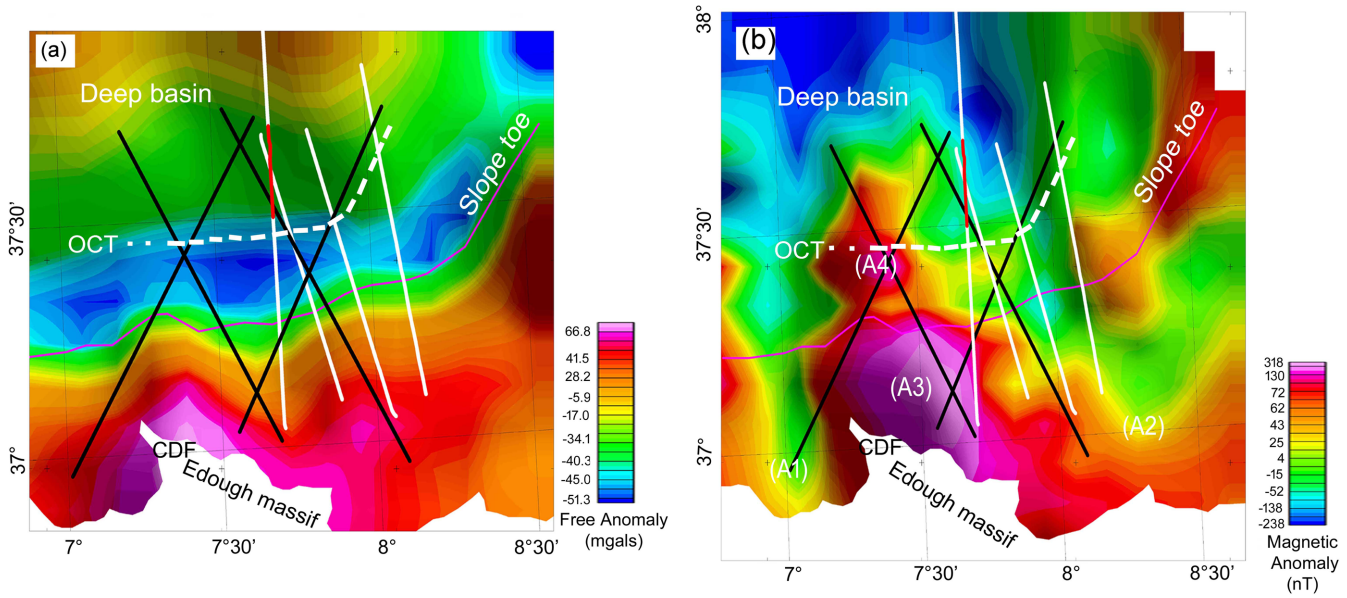

Figure 13. (a) Gravity map (free air anomaly) and (b) magnetic anomaly map reduced to pole in the study area. White lines: gravity and magnetic data acquired during SPIRAL cruise. Black lines: additional available data. Purple line: slope toe location (see also Fig. 2b). Red line: location of the local overthickening of the basement units observed along the *P*-wave velocity–depth model. White dotted line (OCT): ocean-continent transition zone after this study. CDF: Cap de Fer.

comparisons of the picked/computed travel-times were made, to determine the interface of the model along which the *P*-wave to *S*-wave conversions occurred. For each tested interface, the Poisson's ratio and related *S*-wave velocity were changed, until a satisfactory fit between the computed and observed travel-times was obtained.

The *P*-wave to *S*-wave conversion interface is known to be associated with high impedance contrast (White & Stephen 1980), which is usually provided by the seabed, the top of the salt layer, or the top of the oceanic crust, so each of these three interfaces was tested. Whatever the conversion interface was, the ray tracing indicated that the observed *S*-waves traveled down to the deepest layers of the LC and UM models (Fig. 12b). Based on the *P*-wave velocity within the upper mantle UM ($\geq$8.0 km s^{-1}), we considered a constant Poisson's ratio of 0.25, as usually given for mantle rock at a similar depth (Christensen 1978; Spudish & Orcutt 1980; Purdy 1983; Karson *et al.* 1984; Price & Morgan 2000). For each tested conversion interface, Poisson's ratio values in the crustal layers were tested to adjust the computed to the observed travel-times, and the corresponding *S*-wave velocity was determined.

These tests demonstrate clearly that conversion at the seabed leads to unrealistic values of the Poisson's ratio in the LC of $\sim$0.24, which falls without the bounds defined for crustal rock (Christensen 1978; Spudish & Orcutt 1980; Purdy 1983; Karson *et al.* 1984; Price & Morgan 2000). No value of the Poisson's ratio was found to successfully model the *S*-wave travel-times. Indeed, the best fit was finally obtained for a conversion that occurred at the top of the Messinian salt layer (Fig. 12b). This result is consistent with our observation of the *S*-wave only where the Messinian salt layer is thick in the deep basin (Fig. 5), and with previous studies that indicated that the top of the salt layer is a good candidate for this kind of conversion in the Mediterranean basin (Lelgemann & Klaeschen 1999) and elsewhere (Ogilvie & Purnell 1996). This is probably because this interface is associated with a high impedance contrast, as required for this type of conversion (White & Stephen 1980).

With a *P*-wave to *S*-wave conversion occurring at the top of the salt layer, the travel-times and the offsets of the *S*-waves were best reproduced for a Poisson's ratio of 0.28 (Fig. 12c) and an average Vs of 3.6 km s^{-1} in the LC layer. For these values, the RMS travel-time misfit was 0.162, and χ^2 was 6.347. For a perturbation of 0.02 (7.2 per cent) of the Poisson's ratio in the LC, the percentage of the modelled picks decreased significantly (Fig. 12c). We thus estimate the final value of the Poisson's coefficient in the LC to be 0.28 $\pm$ 0.1.

4.4 Gravity and magnetic maps

The free-air-anomaly gravity map shows values from $-$57 mGal to $+$87 mGal (Fig. 13a). The map in Fig. 13a shows two E-W elongated positive anomalies: the first marks the continental shelf and the adjacent continental slope, with greater than $+$80 mGal offshore of the Edough Massif (Fig. 13a); the second one is within the deep basin north of 37°36′N. Between these two positive anomalies, a set of negative anomalies with values lower than $-$50 mGal mark the edge of the deep basin, just north of the slope toe. This set consists of three E-W to NE-SW trending anomalies and it appears to extend further to the NE.

The magnetic anomaly map shows values from $-$238 nT to $+$318 nT (Fig. 13b). This map shows several long-wavelength anomalies (extension, $\geq$25 km). Two negative anomalies, A1 and A2, with values from $-$52 nT to $+$13 nT and from $-$52 nT to $+$54 nT, respectively, correspond to the Skikda and Annaba Bays. Between these two negative anomalies, there are two positive anomalies, A3 and A4, with values from $+$95 nT to $+$318 nT. The A3 anomaly corresponds to the dome-like part of the continental slope that was observed offshore of Cap de Fer (Fig. 13b). In the northern part of the study area, the deep basin is characterized by negative anomalies, from $-$100 nT to $-$238 nT. These negative values sharply increase to positive ones along a NS trending corridor located at $\sim$8°E, west of the Sardinia Channel.

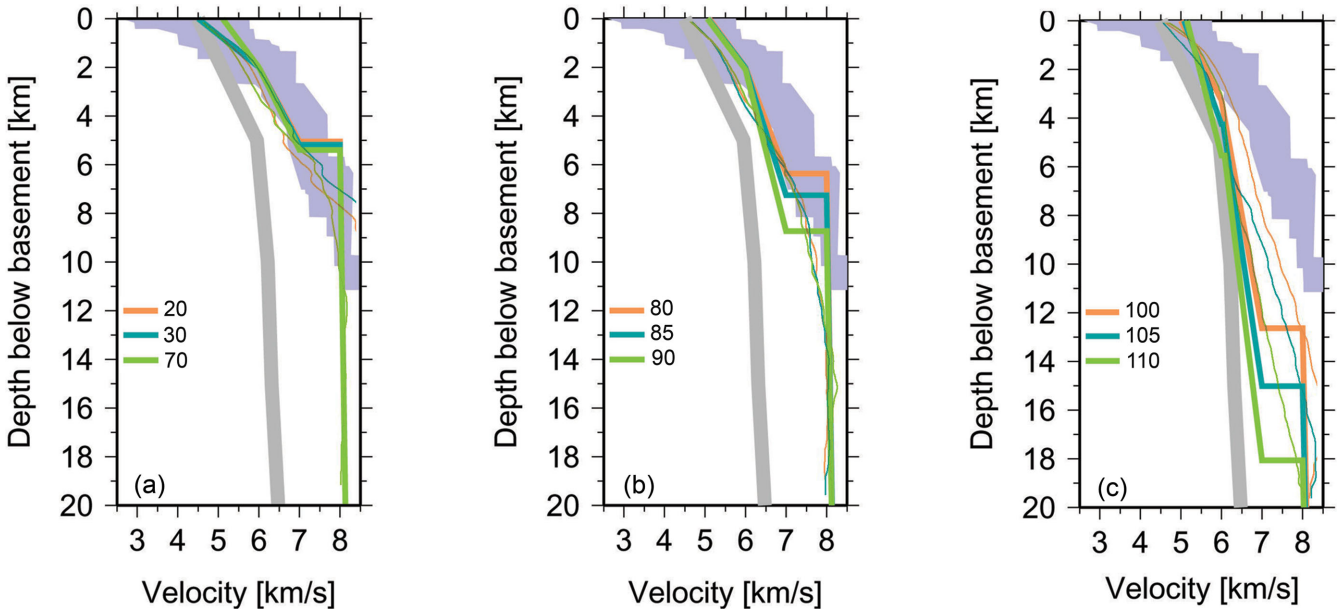

Figure 14. 1-D velocity–depth profiles in the basement and upper mantle extracted from the *P*-wave velocity–depth models along line WA-An, compared to 1-D velocity–depth profiles computed in other geodynamic contexts. Coloured lines: 1-D velocity–depth profiles extracted from the forward velocity–depth model (thick lines) and from the tomographic velocity–depth model (thin lines). Location along the velocity–depth model is given in km on the left-hand side of the diagrams. Grey areas: compilation for extended continental crust from Christensen & Mooney (1995). Blue areas: compilation for Atlantic oceanic crust from White *et al.* (1992). (a) From the northern end of the profile up to ∼75 km in the velocity–depth model (Fig. 11), the velocity laws are situated within the bounds of oceanic crust. (b) Between ∼75 and ∼95 km in the velocity–depth model (Fig. 11), the velocity laws are intermediate between continental and oceanic velocity laws. Finally, between ∼95 km and the southern end of the velocity–depth model (Fig. 11), the velocity laws are within the bounds of continental crust.

5 DISCUSSION

The velocity–depth model computed from forward modelling can be split into three domains that show distinct velocity–depth features. Comparison of the 1D velocity–depth profiles extracted from underneath the basement for each of these three domains (White *et al.* 1992; Christensen & Mooney 1995) help to define the extent of each of the domains of different nature of the crust along the wide-angle profile (Fig. 14). For the tomographic model the vz-profiles were extracted underneath the 4.5 km s^{-1} isocontour, which then represents basement. Subsequently the discussion is extended throughout the study area, using the interpretation of the seismic reflection lines, which are crucial to discuss the nature and origin of the margin sediment and the lateral changes in the margin structure and in the continent transition location. Finally, we propose a scenario for the geodynamic evolution of the eastern Algerian margin and its adjacent basin that is deduced from these new results.

6.1 Structure of the deep basin

6.1.1 Southward thickening of the sediment

In the northern part of the model, the sedimentary cover of the deep basin shows an ∼3-km thickness that increases to ∼5 km at the foot of the margin (Fig. 11). The seismic reflection data indicated that in detail, the thickening was gradual for the post-MSC units, and was sharp in the ∼15 km area bounding the slope toe for the Pre-MSC unit. Here, the local over-thickening of the Pre-MSC unit is underlined by a continuous negative gravity anomaly that reaches minimum values of ∼50 mGal (Fig. 13a). The large-scale southward increase in the sediment thickness that was already observed in the 1970's all along the Algerian margin had been interpreted as the result of lithospheric bending related to the Algerian margin contractive reactivation (Auzende *et al.* 1972; Auzende *et al.* 1975). Near the margin, the short wavelength over-thickening can be partly explained by thrusts related to the margin reactivation (Kherroubi *et al.* 2009). However, over-thickening was still observed a few kilometers north of the reactivated area, where the Pre-MSC unit is not deformed. This might be due to the presence of Oligocene sediment that contributed to the thickening of the Pre-MSC unit, and also to higher rates of Miocene subsidence along the margin toe (Arab *et al.* 2014). The easternmost part of the study area (Fig. 6, Line Spi21) is an exception, as the Pre-MSC unit is thinner here than elsewhere, above a shallower basement marked by an increase in the gravity anomaly values (Fig. 13b).

6.1.2 A thin magmatic oceanic crust

From the northern end of the profile up to 75 km (Fig. 11, oceanic domain), the crust is modelled using two layers. The shallowest layer, UC, is 2.2 km thick, with velocities from 4.8 km s^{-1} to 6.0 km s^{-1}, while the deepest, LC, is 3.3 km thick, with velocities from 6.0 km s^{-1} to 7.1 km s^{-1}. These velocity values are situated within the bounds of the oceanic crust, as compiled by White *et al.* (1992) for the Atlantic Ocean (Fig. 14a). However, except between 40 km and 60 km, the crust is ∼5.5 km thick, thinner than the typical oceanic crust, which usually has a thickness of 7 km (White *et al.* 1992). Nevertheless it is consistent with the oceanic crust thickness in other parts of the western Mediterranean Sea (Hinz 1973; Vidal *et al.* 1998; Contrucci *et al.* 2001; Gailler *et al.* 2009; Grevemeyer *et al.* 2011; Leprêtre *et al.* 2013; Mihoubi *et al.* 2014) as compiled by Gailler *et al.* (2009, Fig. 15a). The velocity-depth

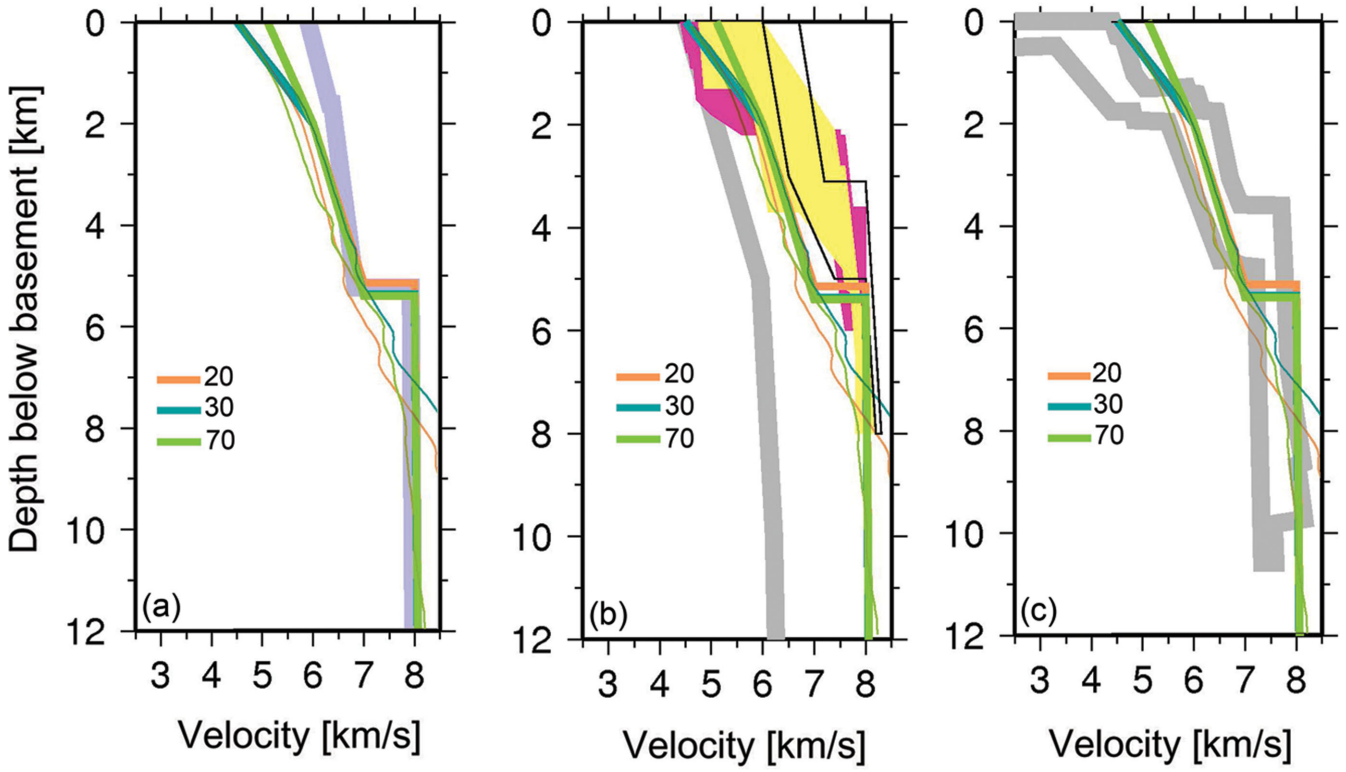

Figure 15. 1-D velocity–depth profiles in the basement and upper mantle extracted from the forward *P*-wave velocity–depth model (thick coloured lines) and from the tomographic velocity–depth model (thin coloured lines) in the oceanic domain along line WA-An, compared to 1-D velocity–depth profiles computed in other geodynamic contexts. (a) Blue area: compilation for oceanic crust in western Mediterranean, offshore Sardinia, from Gailler *et al.* (2009). (b) Compilation of velocity laws computed for seismic crusts mainly composed by more or less altered peridotites. Pink area: compilation for ocean-continent transition zone in the southern Iberia Abyssal from Dean *et al.* (2000). Yellow area: compilation for rifted margin of the eastern Grand Banks of Newfound land (Canada) from van Avendonk *et al.* (2006). Transparent area: compilation for the western Iberia passive continental margin from Afilhado *et al.* (2008). (c) White area: compilation for Mohns Ridge oceanic crust, created along a slow but hot spreading ridge (Klingelhoefer *et al.* 2000).

profiles extracted from the tomographic model indicate a similar crustal thickness, with a sharp increase of the velocity gradient representing the Moho from 70 to 20 km model distance. Between 80 and 90 km model distance the velocities from the tomographic model do not image the Moho discontinuity but closely follow the same gradient as the forward modelled ones. This can be explained by the lack of arrivals reflected at the crust-mantle boundary in the tomographic model.

An abnormally thin oceanic crust is frequently associated with processes of oceanic floor creation that are dominated by tectonic extension rather than by magmatic accretion, either due to very slow accretion rates (Jackson *et al.* 1982; Minshull & White 1996; Grevemeyer *et al.* 1997; Jokat & Schmidt-Aursch 2007), or to an abnormally cold accretion context, like along intra-oceanic fracture zones or transform margins (Fox & Gallo 1984; White *et al.* 1984; Sage *et al.* 1997) or along ocean-continent transition during the earliest phases of ocean spreading (Whitmarsh *et al.* 1996; Nicholls *et al.* 1981). In these cases, the seismic crust often includes altered peridotites, and presents specific velocities and thicknesses, as illustrated by the examples compiled in Fig. 15b. Crustal velocities range from 5.0 km s^{-1} to 5.5 km s^{-1}, and from 7.8 km s^{-1} to 8 km s^{-1}, with the velocity controlled by the degree of serpentinization that decreases with increasing depths (e.g. Christensen 1966; Francis 1981; Minshull *et al.* 1991). Velocities of the order of 7.5 km s^{-1} or more are systematically found at the base of the seismic crust. The crust is modelled by a 4.0-km thick to 5.0-km-thick layer (Dean *et al.* 2000; van Avendonk *et al.* 2006; Afilhado *et al.* 2008; Prada *et al.* 2014; Fig. 15b). This thickness corresponds to the maximum depth reached by the hydrothermal circulation that is responsible for serpentinization of the upper mantle material (Francis 1981; Minshull *et al.* 1991; Chian *et al.* 1999; Dean *et al.* 2000). In the Annaba area, the distinct velocity gradients within the two crustal layers (0.55 km s^{-1} and 0.33 km s^{-1}, for the UC and LC, respectively), and the absence of velocities greater than 7.1 km s^{-1} at the base of the seismic crust, suggest that although the crust is thinner than the normal oceanic crust, it is not dominantly composed of altered peridotites.

The Poisson ratio provides further arguments to discuss the nature of the crust. The value of the Poisson ratio in the Annaba area is constrained to be ~0.28 in the LC. This value falls within the bounds given for gabbroic rock (Carlson & Miller 1997), but out of the bounds given for altered peridotites (Miller & Christensen 1997), even if pure gabbro and peridotites with 10 per cent to 20 per cent serpentinites can show similar Poisson's ratios at *P*-wave velocities of 6.1 km s^{-1} to 7.2 km s^{-1} (Horen *et al.* 1996). These data strongly suggest that the nature of the lower oceanic crust offshore of Annaba is dominantly magmatic, and composed of gabbroic rock rather than of peridotites, even if small amounts of more or less altered mantle rock cannot by excluded. The crustal 1D velocity–depth profile in the Annaba deep basin is very similar to that modelled for Mohns Ridge (Fig. 15c). Here, geochemical data were combined with the results of wide-angle modelling to show that the oceanic crust is abnormally thin, but composed of a continuous magmatic crust, made of gabbro and basalt (Klingelhoefer & Géli

2000; Klingelhoefer *et al.* 2000). In this case, slow but hot accretion processes have led to low but steady magmatic production, which explains the abnormal crustal thickness.

The WA-Ji profile is located 170 km westward of the Annaba profile WA-An (Mihoubi *et al.* 2014), and it crosses the area of the eastern Algerian basin that is characterized by the regular, NW-SE-trending magnetic anomaly set that extends to the margin toe offshore of Jijel (Fig. 1a). Here, the regular anomaly pattern suggests a period of continuous and steady magmatic accretion, in contrast with other parts of the western Mediterranean Sea. Although the study area is located just south of this regular set of magnetic anomalies (Fig. 1a), the velocity-depth model computed offshore of Annaba is very similar to that computed offshore of Jijel, in terms of the velocity and thickness of the oceanic crustal layers (Mihoubi *et al.* 2014). Both models are consistent with a Mohns-like crustal structure and accretion style. In detail, the velocity gradients plotted along the tomographic model in the Annaba area show a slight, lateral variability of the crustal velocity. Although forward wide-angle seismic models of the Annaba and Jijel regions are very similar to first order, the complex magnetic patterns of the magnetic anomalies and the variable velocity gradients suggest a slightly more heterogeneous magmatic crust and related accretion processes in the Annaba region than in the region characterized by the regular magnetic anomaly pattern.

Between ∼40 km and ∼65 km along the model, a crustal over-thickening of 2 km can be observed for both the tomographic and the forward velocity–depth models (Figs 8 and 11), which corresponds to a relief involving the Pre-MSC reflectors along the coincident MCS line (Fig. 5). The magnetic profile recorded along the wide-angle line clearly shows a positive anomaly related to this over-thickening (Fig. 11), whereas it is not related to a specific anomaly on the magnetic and gravity maps (Figs 13a and b). This suggests that the over-thickening is a local feature that may be interpreted as magmatic in origin.

This crustal magmatic over-thickening might be explained by syn-expansion of magmatic intrusion that was emplaced within the backarc basin, as described for the Ligurian Sea (Rollet *et al.* 2002), where volcanoes of similar extent have been described. It can alternatively be explained by post-collisional magmatism related to slab break-off, as proposed for the magmatic bodies described onshore (Maury *et al.* 2000; Caby *et al.* 2001; Laouar *et al.* 2005). The two MCS lines crossing this structure show that Pre-MSC reflectors above the crustal thickening are inclined outward of the structure (Fig. 5), regardless of the profile orientation. Such geometry is compatible with a Miocene magmatic phase, which would have occurred prior to the Messinian event, as shown by the overlaps of the Messinian reflectors at the top of the Pre-MSC unit.

6.2 Margin structure

6.2.1 A stretched continental margin

From 95 km to the southern end of the profile (Fig. 11, continental domain), the velocities can be correlated with those for the thinned continental crust from a compilation proposed by Christensen & Mooney (1995). Along the wide-angle seismic profile, the continental basement progressively rises from below the margin, to outcrop near the coast (Fig. 11); this is in agreement with the outcrop of the Edough Massif that represents the crystalline basement immediately along the shoreline (Fig. 2a). The internal/external zone thrust boundary that is crossed by the wide-angle seismic line north of the Edough Massif (Fig. 2a) is not resolved in our velocity–depth model. This might be explained as the suture zone probably brings two crystalline basements into contact with little velocity contrast, but also by poor resolution of the velocity–depth model for its continental part due to the absence of reverse shots. Lack of constraints results here in a slightly different velocity repartition in the tomographic and the forward model, even though they both allow a good fit of the modelled and observed travel times. Indeed, similar travel times are modelled in the forward model by laterally homogenous velocity in UC and LC, and along the tomographic model by a local lateral lowering of the crustal velocity compensated in depth by a ∼3-km continental ward shift of the Moho that is also slightly steeper (Fig. 8). Because of this discrepancy, the detailed distribution of the *P*-wave velocities within the continental crust cannot be interpreted. However, the tomographic and forward velocity models both show a gradual deepening of velocities higher than 6.5 km s^{-1} under the continental slope, indicating a gradual crustal thinning of ∼15 km over an ∼35-km distance between the Edough Massif on-land and the margin toe (Fig. 11). The margin is narrow compared to most of the continental rifted margins (e.g. Crosby *et al.* 2011, and references therein). However, this is similar to other Mediterranean rifted margins, such as the northern Liguria margin (Contrucci *et al.* 2001; Rollet *et al.* 2002; Dessa *et al.* 2011), and the western Sardinia margin (Gailler *et al.* 2009).

Compared to other sections of the Algerian margin, the Annaba margin is the only one that has a typical stretched margin structure. In the Jijel area (Fig. 1a, Line WA-Ji), the crustal thinning is gradual for the LC, while it is sharp for the UC, which shows an ∼7-km thinning over less than 4 km in distance (Mihoubi *et al.* 2014). This geometry can be explained by oblique rifting that led to heterogeneous thinning of the different crustal levels (Mihoubi *et al.* 2014). In the Tipaza area, which is located ∼450 km west of our wide-angle seismic line (Fig. 1a, Line WA-Ti), a narrow zone of crustal thinning was proposed to have resulted from a late transcurrent episode connected with the westward migration of the Alboran domain, which cut through the distal part of the rifted margin formed in an earlier stage of the evolution of the Algerian basin (Leprêtre *et al.* 2013; Medaouri *et al.* 2014). Finally, in the Mostaganem area (Fig. 1a, Line WA-Mo), there is sharp thinning of the continental crust of 10 km over a 10-km distance, which is interpreted as depicting a STEP-fault that was formed along the westernmost part of the Algerian basin, due to the slab retreat of the Alboran subduction (Badji *et al.* 2015). Thus the structure of the northern Algerian margin appears to be segmented due to its geodynamic evolution that differs from one place to another. In this complex context, the Annaba segment shows the preserved structure of the stretched southern margin of the backarc basin opened at the rear of the AlKaPeCa forearc.

6.2.2 A variable crustal thickness along the eastern margin

The AlKaPeCa blocks outcrop in the Edough Massif, where they reaches ∼1000 m in elevation along the northern side of the suture zone (Fig. 2b), and then disappear eastward below the flysch to outcrop again in the Galite Island, offshore of Tunisia (Fig. 1a) (Tricart *et al.* 1994; Bouillin *et al.* 1998; Mascle *et al.* 2004; Belayouni *et al.* 2010). Between these basement outcrops, the basement top is ∼4 km deep in the Annaba Bay area, and is buried below the Pre-MSC and PQ sedimentary units. If we assume that the Moho depth compensates for the surface topography, as suggested by the velocity–depth model that crosses the Edough Massif, this lateral change in the basement top topography indicates that the AlKaPeCa crust is much thinner in the Annaba Bay area than in the

Edough area or in the Sardinia Channel (Peirce & Barton 1992). In the Annaba Bay area, the suture zone is expected to be located offshore (Fig. 2a). The internal zones should reach their maximum thickness north of this. A thin continental crust north of the suture zone implies that the AlKaPeCa forearc was thinned in the Annaba Bay area before its collage to the African margin.

6.2.3 Record of the Miocene margin evolution by the Pre-MSC sediment

Above the continental basement, the velocity–depth model images a pre-Messinian sedimentary layer that exceeds 2 km in thickness below the slope (Fig. 11, Pre-MSC). The reflection seismic data show that the upper part of these sediments corresponds to the deformed sub-units Fb-Fc, the interpretation of which is discussed in the following paragraph.

The deformation of the Fb unit is pre-Messinian in age, as indicated by the Fb-reflector truncation along the MES (Figs 5 and 7b). Considering the evolution of the Algerian basin, two interpretations can be proposed:

(1) The Fb, Fc and Mio units might correspond to the Oligo-Miocene sediment deposited on the northern flanks of the AlKaPeCa blocks, including the syn- to post-rift sediments. In this hypothesis, they thus correspond to autochthonous sediment that includes a lateral equivalent of the Oligo-Miocene Kabylian units that outcrop onshore in the Kabylian area (Rivière *et al.* 1977; Bouillin 1979; Géry *et al.* 1981; Djellit 1987; Bracene 2001), and the southern continuity of the Pre-MSC units that are observed within the deep basin. In this case, the deformation observed that includes folds and thrusts might have been acquired during the collision of the AlKaPeCa blocks with the African margin. However, in this case, the clear unconformity interpreted as a major tectonic contact between the Fb/Fc and Mio units becomes difficult to explain.

(2) The Fb and Fc units might alternatively correspond to the allochthonous flysch unit that was back-thrust on the AlKaPeCa blocks during the collision. Such back-thrust flysch is known for Greater and Lesser Kabylia, where it corresponds to stacked and deformed units of flysch of various ages (Durand-Delga 1969; Vila 1980; Wildi 1983; Bouillin 1986; Djellit 1987; Bracene & Frizon de Lamotte 2002).

The extension and thicknesses of the Fb-Fc subunits, and their structural relationships, are compatible with the flysch outcrops described onshore (Vila 1980; Djellit 1987). These outcrops show various lithologies of marine clastics. The grain-size of the strata is either contrasted within stratified subunits, or it is very homogenous (Vila 1980). Their deformation varies from one subunit to another, from low levels of deformation that involve monoclinal, low-dipping strata, to high levels of deformation that involve thrusts, folds and verticalization of the strata. We thus propose that below the margin, the Fb subunits can be explained by the relatively low deformation rates and the contrasted lithology of the strata, whereas the Fc subunits can be explained by higher levels of deformation and/or homogenous lithology. Where the Fc subunits lie just above Mio, this might also correspond to soft sediments that were deposited along the margin before the collision, and then subsequently dragged and reworked by the flysch emplacement during the collision.

For this interpretation, the Mio unit corresponds to syn- and post-rift sediments that were deposited over the AlKaPeCa blocks during the evolution of the backarc basin, and afterward possibly deformed during the collision. It should be noted that we do not know of any lateral equivalent of these Fb-Fc subunits elsewhere along the Algerian margin (offshore), which means that these thick and well-organized allochthonous nappes might be restricted to the eastern end of the Algerian margin.

The seaward extension of the deformed Fb-Fc allochthonous units below the slope is uncertain, mainly because recent faults that have been attributed to margin reactivation (Kherroubi *et al.* 2009) have disrupted the unit organization below the deep slope (Fig. 7a). These allochthonous nappes do not extend to the deep basin in this part of the Algerian margin, as at the basin edge, the sub-horizontal geometry of the pre-Messinian deposits is generally in lateral continuity with the deep basin sediment (Figs 5 and 7a).

The dataset does not show any continuity of the Fb unit into the western margin segment that is characterized by the rough morphology (Fig. 2b). Here, the few reflectors observed just below the Messinian surface (Fig. 7c) might correspond either to a lateral equivalent of the pre-Messinian sediment of the deep basin, and thus to Mio, or to the poorly organized Fc flysch. The total sediment thickness, which is much less than east of Line Wa-An, favors the first hypothesis.

Offshore of the Cap de Fer (Fig. 2b, CDF), the particular morphology of the slope is such that it is marked by a dome-like rounded shape (Fig. 2b, D). This brings to mind the rounded shape of magmatic bodies known onshore along the Algerian margin, such as Cap de Bougaroun, Beni Toufout, El Milia, Filfila, and El Aouana (Vila 1978). It might thus correspond to the magmatic northern offshore extent of Cap de Fer, in agreement with the positive anomalies observed on the gravity and magnetic maps for this position (Figs 13a and b). Along the northern flank of the dome, the unusually high dip of the pre-Messinian reflectors suggests that the pre-Messinian units have been tilted toward the deep basin (Fig. 7c). These observations suggest that in this region, Miocene magmatism deeply modified the margin structure, including the pre-Messinian sediment.

6.3 A sharp ocean–continent transition zone

Between 75 km and 95 km along the line (Fig. 11, OCT), the model depicts intermediate velocities that are greater than in a typical continental crust, but slower than in a typical oceanic crust (Fig. 14b). We associate this domain with the ocean–continent transitional zone (OCT). In the Annaba region, the width of the OCT is 20 km, which is similar to that in the Jijel area (Mihoubi *et al.* 2014), but greater than that in the Tipaza area (Leprêtre *et al.* 2013) and the Greater Kabylia area (Aïdi *et al.* 2013), where it is of the order of 10 km wide. This OCT is narrow when compared to most of the other western Mediterranean margins: ~90 km in the Gulf of Lions (Gailler *et al.* 2009); 35 km to 40 km along the northern Liguria margin (Rollet *et al.* 2002; Dessa *et al.* 2011); and 40 km along the western Sardinian margin (Gailler *et al.* 2009). The OCT domains that bound the rifted margins are alternatively explained by: (1) serpentinized mantle, which is mechanically exhumed in the continental rupture area (Beslier *et al.* 1995; Brun & Beslier 1996; Chian *et al.* 1999; Dean *et al.* 2000); (2) oceanic crust that is accreted at slow or very slow accretion rates and is rich in mantle rock and exhumed gabbros (Whitmarsh *et al.* 1996); or (3) stretched continental crust, that is fractured and intruded by magmatic material (Whitmarsh & Miles 1995). However, in these three cases, *P*-wave velocities greater than 7.5 km s^{-1} are systematically modelled at the base of the crust (Whitmarsh & Miles 1995; Whitmarsh *et al.* 1996; Funck *et al.* 2004; Klingelhoefer *et al.* 2005). The nature of these OCT thus

differs from that offshore of Annaba, where the Moho is characterized by a sharp velocity increase, from 7.1 km s^{-1} to 8.0 km s^{-1}.

The detailed interpretation of a dense net of reflection seismic lines along the basin edge indicates that the thick pre-Messinian sediment observed along the deep basin southern edge includes syn-rift sediment (Arab *et al.* 2014). In this area, the 10-km-wide bathymetric step observed along the deep basin edge (Fig. 5) would thus belong to the continental domain, although this block is located within the OCT in our velocity–depth model (Fig. 11). Indeed, the OCT domain defined in the velocity model might represent the area across which the crustal turning rays cross both the continental and oceanic edges, as this area is modelled by averaged continental and oceanic velocities. The OCT could thus be much narrower than 20 km, located along the northern edge of the bathymetric step. Following Arab *et al.* (2014), the OCT along the eastern Algerian margin might be located north of the over-thickened Pre-MSC unit marked in our dataset by both a strong negative gravity anomaly (Fig. 13a), and the lateral change in the Messinian salt deformation style. In the easternmost part of the study area, along Line Spi21 (Fig. 6), the OCT would locate further to the north, 35 km from the margin toe, thus implying a northward inflexion of the OCT east of the study area (Fig. 2a). This inflection marks the transition to the continental domain of the Sardinia Channel, where wide-angle seismic modelling indicates a 10-km-thick to 25-km-thick continental crust (Fig. 1a; Peirce & Barton 1992). The easternmost part of the study area would thus be part of the continental Sardinia Channel.

6.4 Implication for kinematic models

In the study area, the geophysical dataset presented above brings new constraints to the structure of the eastern Algerian basin and its southern continental margin. The data interpretation strongly suggests that the offshore domain in the Annaba area corresponds to a rifted margin segment that separates the internal zones to the south, here represented by the Edough Massif, from the deep eastern Algerian oceanic basin to the north. Below the eastern segment of the margin, we interpret the burying of the continental basement top as a marker of the longitudinal thinning of the AlKaPeCa blocks between the Edough Massif and the Sardinia Channel before the collision. In the same area, a thick sequence of flysch units might have been back-thrust over the margin. North of the margin, a regular magnetic anomaly pattern that is observed in the centre of the eastern Algerian basin characterizes a period of steady oceanic accretion. The velocity–depth models offshore of Jijel and Annaba were similar to first order, and they indicate that in the regular anomaly pattern area, and south of it, the eastern Algerian basin is characterized by a thin oceanic crust that is dominantly composed of magmatic rock, thus recalling the crustal structure of the Mohns Ridge formed in a slow but hot context. These results open new insights into the kinematic models proposed to date for the evolution of the eastern Algerian basin and the adjacent margin.

The two-step kinematic models proposing that the regular magnetic pattern was created after the southeastward migration of the AlKaPeCa blocks imply accommodation of the newly created oceanic space to the west, either by subduction (Cohen 1980), or along a transform zone along the eastern Algerian margin (Mauffret *et al.* 2004). On the one hand, a fossil subduction trench along the western edge of the anomalies would be marked by an anomalous depth of the oceanic basement and an anomalous sediment thickness and deformation that have never been described in previous studies (Schettino & Turco 2006; Mauffret 2007; Mihoubi *et al.* 2014). On the other hand, transform zones are characterized by a sharp thinning of the oceanic crust that tends to be a-magmatic, over a width of 30 km to 40 km (Fox & Gallo 1984; White *et al.* 1984; Minshull *et al.* 1991). In velocity–depth models, this consists of a 2-km-thick to 4-km-thick crust with velocities from ∼5 km s^{-1} to 7.8–8.0 km s^{-1} from top to bottom (Cormier *et al.* 1984; White *et al.* 1984; Potts *et al.* 1986; Minshull *et al.* 1991), a structure that is not imaged in the Jijel velocity–depth model (Mihoubi *et al.* 2014) and the Annaba velocity–depth model.

The one-phase, Gelabert-type kinematic model (Gelabert *et al.* 2002) that proposed gradual oceanic opening accompanied by southeastward arc migration appears to better account for the basin crustal structure. This model implies that during the opening stage, (1) an asthenospheric rise filled the void caused by arc migration, and (2) the trend of the spreading centre axis, as given by the NW-SE magnetic anomaly pattern, was more or less perpendicular to the subduction trench (Fig. 16b), which is an unusual configuration. Indeed, the expected and observed direction of backarc extension and/or accretion along the ocean/continent subduction zones is more or less parallel to the trench direction, whatever the driving force of the backarc opening is (slab pull effect: e.g. Malinverno & Ryan 1986; Royden 1993; mantle flow in the asthenospheric wedge overlying the slab: e.g. Rodkin & Rodnikov 1996; or extrusion processes: e.g. Tapponnier *et al.* 1986; Mantovani *et al.* 2001). Only a few examples related to specific kinematic contexts show rifts or spreading centres running perpendicular to the trench. This is the case where the convergence direction is oblique to the subduction zone, which leads to strain partitioning and lateral escape of the continental edge, and subsequent basin opening (e.g. Andaman Sea: Diehl *et al.* 2013; California Gulf: Karig & Jensky 1972).

In the case of the eastern Algerian basin, the geometry of the backarc accretionary system is thus an exception. This can be explained by the evolution of the trench geometry that gradually passed from linear, or slightly arcuate, to cubit (Figs 16a and b), as the Corso-Sardinia and the Kabylian blocks migrated eastward and southward, respectively (Gelabert *et al.* 2002). Numerous kinematic reconstructions propose that the Alpine collision along the African margin was followed by the eastward migration of the slab and the related opening of the Tyrrhenian basin (e.g. Carminati *et al.* 1998; Spakman & Wortel 2004). This implies the tear of the slab below the Sardinia Channel and the southern edge of the Tyrrhenian Sea, as the slab retreated eastward. We propose that this slab tear occurred earlier, during the migration of the AlKaPeCa blocks, due to the divergent directions of the slab retreat, as eastward east of the Corso-Sardinia block, and southward south of the Kabylian blocks (Fig. 16b), following the model of the double saloon door geometry proposed by Martin (2006). Slab tear faults open asthenospheric windows and are thus associated with thermal anomalies responsible for anomalous magmatic processes in the overlying lithosphere (Keskin 2003; Faccenna *et al.* 2005; De Asti *et al.* 2006; Rosenbaum *et al.* 2008). In the context of the Miocene backarc opening of the eastern Algerian basin, we propose that abnormally hot oceanic accretion could have occurred just above the tear fault. In particular, such warmer accretion might have led to the production of a thin but magmatic crust along a 200-km-long spreading centre, thus leading to more continuous magma production, compared to the other western Mediterranean sub-basins.

To the south, the oceanic opening was necessarily accompanied by longitudinal, E-W extension of the AlKaPeCa blocks along the forearc, before the collision (Fig. 16b). This extension can be accommodated either by extensional or transcurrent deformation, as

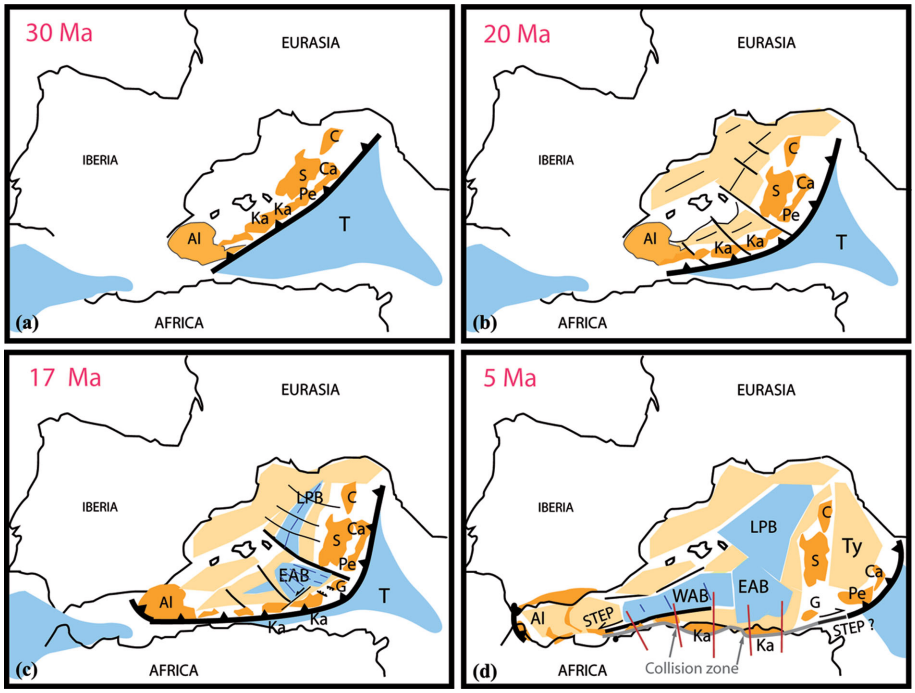

Figure 16. Kinematic reconstruction of the eastern Algerian basin between 30 and 5 Ma, in the context of the western Mediterranean evolution. (a) 30 Ma. The AlKaPeCa block forms the European forearc at the southern Eurasian continent, along the Tethyan subduction zone that presents a linear shape (b) 20 Ma. Due to the rollback process, the AlKaPeCa and Corso-Sardinia blocks migrate southward and south-eastward as a rifting stage occurs in backarc position at the rear of these blocks. (c) 17 Ma. As the AlKaPeCa blocks migrate to the south and to the southeast, the forearc elongates along the subduction zone that becomes even more arcuate. Related to this arcuate shape, a NW–SE slab tear may emplace below the eastern Algerian basin, opening an asthenospheric window that causes a positive thermal anomaly. Above it, the thin but magmatic oceanic crust of the Eastern Algerian Basin forms along a NW–SE spreading centre. The creation of the oceanic domain is accommodated at its southern edge by extensive and/or transcurrent deformation of the forearc along the free edge of the subduction. Between 17 and 15 Ma, the collision between the Kabylian blocks and the African edge occurs. After the collision, two STEP-faults may develop as slab tears propagate to the west along the western Algerian margin and below the Alboran domain, and to the east along the southern edge of the opening Tyrrhenian domain. (d) 5 Ma. Oceanisation of Tyrrhenian basin begins. Al, Alboran; Ca, Calabrian; C, Corsica; EAB, eastern Algerian basin; G, Galite Island; Ka, Kabylia; LPB, Liguro-Provençal basin; Pe, Peloritani; S, Sardinia; T, Tethys; Ty, Tyrrhenian Sea; WAB, western Algerian basin; red lines, location of the SPIRAL wide-angle seismic lines. The kinematic reconstruction of the western Algerian basin is from Medaouri *et al.* (2014) and reference therein.

presently observed along the Aegean arc (ten Veen & Kleinspehn 2003; Marsellos *et al.* 2010; Kokinou *et al.* 2012). It may explain the crustal thinning of the continental crust observed north of the suture zone in the study area, between Edough Massif and Galite Island. In this area, the basement topography that was low at the time of the collision might have favored the emplacement of thick sequences of flysch units on the internal zones, which are today preserved below the upper margin, as no relief could prevent the flysch back-thrusting to the north (Fig. 16c).

The kinematic model proposed above explains why there is no STEP-fault along the southern edge of the eastern Algerian margin, in contrast with the western Algerian margin (Medaouri *et al.* 2014; Badji *et al.* 2015). Indeed, west of Algiers, the narrow western Algerian basin opened more or less parallel to the margin (Fig. 16c) after the collage of the European forearc to the African margin. This led to the development of a STEP-fault together with the westward slab retreat (Fig. 16c). In contrast, in the case of the eastern Algerian basin, the surface expression of the slab tear may have been the opening of the oceanic basin rather than a STEP, because the lateral expansion of the European arc remained possible along the subduction free edge before the collision (or at the early beginning of the collision) (Fig. 16b), in agreement with a propagation in opposite directions of a slab tear allowing for the birth of a triangular basin of NW oriented seafloor spreading at this place (Fig. 16b; Gelabert *et al.* 2002; Martin 2006). Indeed, the eastern Algerian basin opening belongs to the pre-Kabylian collision stage, whereas the western Algerian basin and the Tyrrhenian basin opening north of a STEP-faults belongs to the post-collision stage, with a symmetric type evolution on both sides of the collision zone.

7 CONCLUSIONS

New wide-angle seismic data constrained by MCS reflection, gravity and magnetic data have allowed the imaging of the deep structure of the eastern Algerian basin and its southern margin in the Annaba region (easternmost Algeria).

The analysis and modelling of the *P*-waves indicate that the crust of the deep basin in the Annaba area is ∼5.5 km thick and oceanic in nature. Based on *S*-wave modelling and the Vp/Vs ratio, the lower crust is mainly composed of gabbros, thus supporting that the seafloor spreading was mainly controlled by magmatic accretion. Comparison of the basin crustal velocity structure with that observed in other studies suggests some similarities with the oceanic crust produced along slow but hot spreading centres.

Below the continental slope, the continental margin crust gradually thins from 22 km at the shoreline, to 7 km at the slope toe. This thinning, which is regularly distributed across the upper and lower crusts, characterizes a typical rifted margin. This part of the Algerian margin might thus correspond to a rifted segment that was inherited from backarc opening at the rear of the Lesser Kabylia block, which is here represented by the Edough Massif that now

outcrops along the coast. We also note a probable thinning of the continental crust along the margin, between the Edough Massif and the Sardinia Channel, which implies that the AlKaPeCa forearc thinned locally prior to the collision.

Between the continental and the oceanic domains, the OCT defined in the *P*-wave velocity–depth model is narrow (<20 km) and the base of the crust does not show the high velocities, which suggests a narrow zone across which the seismic rays turn in the adjacent continental and oceanic domains. From the interpretation of the seismic reflection data, we propose that the ocean-continent transition localizes within the deep basin, ∼15 km from the slope toe.

Based on the new crustal structure and the magnetic anomaly pattern of the deep basin, we reviewed the numerous kinematic reconstruction models proposed in the literature for the eastern Algerian basin. We did not find any evidence for a two-step kinematic model that assumes that the eastern Algerian basin opened after the AlKaPeCa/Africa collision. We propose that the central part of the basin that is characterized by well-organized, 200-km-long, NW-SE trending anomalies was formed during the southeastward migration of the AlKaPeCa blocks above the retreating slab. During the oceanic accretion, the spreading centre was orthogonal to the subduction trench. We explain this unusual pattern by divergent directions of the rollback, eastward for the Corsica-Sardinia block, and southward for the Kabylian blocks, probably favored by slab tear at depth. This oceanic opening was probably accompanied by extension along the AlKaPeCa forearc, with this thinning being preserved today along the margin between the Edough Massif and the Sardinia Channel, north of the suture zone. The geometry of the slab retreat differs from that observed along the western Algerian margin, along which the slab tear developed along the ocean-continent transition together with a STEP-fault in the overlying lithosphere.

ACKNOWLEDGEMENTS

The SPIRAL Project was funded by the Centre de Recherche en Astronomie, Astrophysique et Géophysique (CRAAG), Direction Générale de la Recherche Scientifique et du Développement Technologique (DG-RSDT), and Sonatrach (a national oil company), in Algeria, and the Institut Français de Recherche pour l'Exploitation de la MER (IFREMER), Centre National de Recherche Scientifique (CNRS), Institut pour la Recherche et le Développement (IRD), and the Universities of western Britany (UBO), Nice-Sophia Antipolis, and P. and M. Curie Paris 6, in France. The authors would like to thank the captain and crew of the R/V Atalante, as well as the OBS, MCS and land station teams, for their efficient work during the data acquisition. We also wish to acknowledge SONATRACH and Agence Nationale pour la Valorisation des Ressources en Hydrocarbures (ALNAFT, Algeria) for allowing us to use and publish additional geophysical data (seismic lines, gravity and magnetic data). We are grateful to S. Operto for providing the processing sequence applied to the wide-angle data, L. Schenini for assistance in the MCS data processing, B. Mercier de Lépinay for processing of the Maradja/Samra high-resolution seismic data and for kindly providing his scripts, and Y. Thomas for MCS data pre-processing. The authors would also like to thank R. Laouar and D. Saadane for having taken the time to accompany us on the field in the Annaba area to introduce us to the onshore geology, R. Bracene and F. Abbassene for constructive discussions on eastern Algeria, G. Rosenbaum and M.-A. Gutscher for scientific discussions regarding the opening of the eastern Mediterranean basin, and M.-O. Beslier for comments that helped improve the quality of the manuscript. The MCS profiles were processed using Geocluster (CGG Veritas), and Seismic Unix (Stockwell 1999) processing software. The Generic Mapping Tool (GMT) software was used in the preparation of most of the figures (Wessel & Smith 1995). We thank Pr. Louden and an anonymous reviewer for their reviews of the manuscript that allowed significant improvements to be made.

REFERENCES

Afilhado, A., Matias, L., Shiobara, H., Hirn, A., Mendes-Victor, L. & Shimamura, H., 2008. From unthinned continent to ocean: the deep structure of the West Iberia passive continental margin at 38°N, *Tectonophysics,* **458,** 9–50.

Aïdi, C. *et al.*, 2013. Deep structure of the Algerian continental margin in the Great kabylies—insights from wide-angle seismic modeling, AGU2013, T21A-2522. Continental Rifts and Rifted Margins, Posters. CONTROL ID: 1794050.

Alvarez, W., Cocozza, T. & Wezel, F.C., 1974. Fragmentation of the Alpine orogenic belt by microplate dispersal, *Nature,* **248,** 309–314.

Arab, M. *et al.*, 2014. Origin and tectono-sedimentary evolution of the eastern Algerian Basin (offshore) from Upper Oligocene to Present Day, *Basin Research Journal*, BRE-073-2014, in press.

Auffret, Y., Pelleau, P., Klingelhoefer, K., Géli, L., Crozon, J., Lin, J. & Sibuet, J.C., 2004. MicrOBS: a new generation of bottom seismometer, *First Break,* **22,** 41–47.

Auzende, J.M., 1978. Histoire Tertiaire de la Méditerranée occidentale, *PhD thesis,* Paris VII University, 232 pp.

Auzende, J.M., Bonnin, J. & Olivet, J.L., 1975. La marge nord-africaine considérée comme marge active, Art N° 257 - contribution COB N° 338, 681–690.

Auzende, J.M., Olivet, J.L. & Bonnin, J., 1972. Une structure compressive au nord de l'Algérie, *Deep-Sea Res.,* **19,** 149–155.

Avedik, F., Renard, V., Allenou, J. & Morvan, B., 1993. 'Single bubble' airgun array for deep exploration, *Geophysics,* **58,** 366–382.

Badji, R. *et al.*, 2015. Geophysical evidence for a transform margin offshore Western Algeria: a witness of a subduction-transform edge propagator ?, *Geophys. J. Int.,* **200,** 1029–1045.

Belayouni, H., Brunelli, D. & Clocchiatti, R., DiStaso, A., ElHassani, I.A., Guerrera, F. & Kassaa, S., 2010. La Galite Archipelago (Tunisia, North Africa): stratigraphic and petrographic revision and insights for geodynamic evolution of the Maghrebian Chain, *J. Afr. Earth Sci.,* **56,** 15–28.

Berkhout, A.J. & Verschuur, D.J., 1997. Estimation of multiple scattering by iterative inversion, Part 1: theoretical considerations, *Geophysics,* **62**(5), 1586–1595.

Beslier, M.O., Bitri, A. & Boillot, G., 1995. Structure of the ocean continent transition on a passive continental-margin—multichannel seismic-reflection in the Iberia Abyssal-Plain (Portugal), *C. R. A. S., Série II,* **320**(10), 969–976.

Bezada, M.J., Humphreys, E.D., Toomey, D.R., Harnafi, M., Dávila, J.M. & Gallart, J., 2013. Evidence for slab rollback in westernmost Mediterranean from improved upper mantle imaging, *Earth planet. Sci. Lett.,* **368,** 51–60.

Billi, A. *et al.*, 2011. Recent tectonic reorganization of the Nubia-Eurasia convergent boundary heading for the closure of the western Mediterranean, *Bull. Soc. Géol de France,* **182**(4), 279–303.

Boubaya, D., 2006. Etude géophysique multi-méthodes du nord est Algérien: implications sur le lien entre le diapirisme salifère et l'extension de la couverture "thin-skinned extension", in *Mémoire de magister,* USTHB University, Algiers, 140 pp.

Bouillin, J.P., 1979. La transversale de Collo et d'El Milia (Petite Kabylie) : une region-clef pour l'interprétation de la tectonique alpine de la chaîne littorale d'Algérie, in *Mém. Soc. Géol. France,* N.S., LVII, 1978, Mém. N° 135, parution 1979, Paris.

Bouillin, J.P., 1986. Le bassin Maghrébin : une ancienne limite entre l'Europe et l'Afrique à l'ouest des Alpes, *Bull. Soc. Géol. de France,* **8**(4), 547–558.

Bouillin, J.P., D.Delga, M., Gelard, J.P., Leikine, M., Raoult, J.F., Raymond, D., Tefiani, M. & Vila, J.M., 1970. Definition of a Massylian flysches and a Mauretanian flysches in heart of allochton flysches of Algeria, *Comptes Rendus Hebdomadaires Des Séances De L'Académie Des Sciences, Série D,* **270**(19), 22–49.

Bouillin, J.-P., Poupeau, G., Tricart, P., Bigot-cormier, F., Mascale, G. & Torelli, L. l'équipe scientifique embarquée, 1998. Premières données thermo-chronologiques sur les socles sarde et kabylo-péloritain submergés dans le canal de Sardaigne (Méditerranée occidentale), *C. R. A. S., Paris,* **326,** 561–566.

Bracene, R., 2001. Géodynamique du Nord de l'Algérie: impact sur l'exploration pétrolière, *PhD thesis,* Cergy-Pontoise Univertsity, 101 pp.

Bracene, R. & Frizon de Lamotte, D., 2002. The origin of intraplate deformation in the Atlas system of western and central Algeria: from Jurassic rifting to Cenozoic-Quaternary inversion, *Tectonophysics,* **357**(1–4), 207–226.

Bradshaw, A. & Ng, M., 1987. Multiple attenuation by parabolic stack Radon transform: Geo-X Systems internal paper.

Bruguier, O., Hammor, D., Bosch, D. & Caby, R., 2009. Miocene incorporation of peridotite into the Hercynian basement of the Maghrebides (Edough massif, NE Algeria): implications for the geodynamic evolution of the Western Mediterranean, *Chem. Geol.,* **261,** 192–184.

Brun, J.P. & Beslier, M.O., 1996. Mantle exhumation at passive margins, *Earth planet. Sci. Lett.,* **142**(1–2), 161–173.

Caby, R., Hammor, D. & Delor, C., 2001. Metamorphic evolution, partial melting and Miocene exhumation of lower crust in the Edough metamorphic core complex, west Mediterranean orogen, eastern Algeria, *Tectonophysics,* **342,** 239–273.

Carlson, R. & Miller, D., 1997. A new assessment of the abundance of serpentinite in the oceanic crust, *Geophys. Res. Lett.,* **24,** doi:10.1029/97GL00144.

Carminati, E., Lustrino, M. & Dogliono, C., 2012. Geodynamic evolution of the central and western Mediterranean: tectonics vs. igneous petrology constraints, *Tectonophysics,* **579,** 173–192.

Carminati, E., Wortel, M.J.R, Spakman, W. & Sabadini, R., 1998. The role of slab detachment processes in the opening of the western–central Mediterranean basins: some geological and geophysical evidence, *Earth planet. Sci. Lett.,* **160,** 651–665.

Chian, D.P., Louden, K.E., Minshull, T.A. & Whitmarsh, R.B., 1999. Deep structure of the ocean-continent transition in the southern Iberia Abyssal Plain from seismic refraction profiles: Ocean Drilling Program (Legs 149 and 173) transect, *J. geophys. Res.: Solid Earth,* **104**(B4), 7443–7462.

Chikhi Aouimeur, F., 1980. Les rudistes de l'Aptien supérieur de Djebel Ouenza (Algérie, Nord-Est), *PhD thesis,* USTHB University, Algiers, Algeria, 111 pp.

Christensen, N.I., 1966. Elasticity of ultrabasic rocks, *J. geophys. Res.,* **71,** 5921–5931.

Christensen, N.I., 1978. Ophiolites, seismic velocities and oceanic crustal structure, *Tectonophysics,* **47,** 131–157.

Christensen, N.I. & Mooney, W.D., 1995. Seismic velocity structure and composition of the continental crust—a global view, *J. geophys. Res.: Solid Earth,* **100**(B6), 9761–9788.

Cohen, C.R., 1980. Plate tectonic model for the Oligo-Miocene evolution of the Western Mediterranean, *Tectonophysics,* **68,** 283–311.

Contrucci, I., Nercessian, A., Bethoux, N., Mauffret, A. & Pascal, G., 2001. A Ligurian (Western Mediterranean Sea) geophysical transect revisited, *Geophys. J. Int.,* **146**(1), 74–97.

Cope, M.J., 2003. Algerian licencing round may offer opportunity for exploration plays in deep offshore frontier, *Free Break,* **21,** 37–42.

Cormier, M.H., Detrick, R.S. & Purdy, G.M., 1984. Anomalously thin crust in oceanic fracture zones: new seismic constraints from the Kane fracture zone, *J. geophys. Res.,* **89,** 10 249–10 266.

Crosby, A.G., White, N.J., Edwards, G.R.H., Thompson, M., Corfield, R. & Mackay, L., 2011. Evolution of deep-water rifted margins: testing depth-dependent extensional models, *Tectonics,* **30**(1), doi:10.1029/2010TC002687.

De Astis, G., Kempton, P.D. & Peccerillo, A., 2006. Trace element and isotopic variations from Mt. Vulture to Campanian volcanoes: constraints for slab detachment and mantle inflow beneath southern Italy, *Contrib. Mineral. Petrol.,* **151,** 331–351.

Dean, S.M., Minshull, T.A., Whitmarsh, R.B. & Louden, K.E., 2000. Deep structure of the ocean-continent transition in the southern Iberia abyssal plain from seismic refraction profiles: the IAM-9 transect at 40 degrees 20′N, *J. geophys. Res.: Solid Earth,* **105**(B3), 5859–5885.

Dercourt, J. *et al.*, 1986. Geological evolution of the Tethys belt from the Atlantic to the Pamir since the Lias, *Tectonophysics,* **123,** 241–315.

Dessa, J.X. *et al.*, 2011. The GROSMarin experiment : three dimensional crustal structure of the north Ligurian margin from refraction tomography and preliminary analysis of microseismic measurements, *Bull. Soc. Géol. de France,* **182**(4), 305–321.

Déverchère, J. *et al.*, 2005. Active thrust faulting offshore Boumerdès, Algeria, and its relations to the 2003 Mw 6.9 earthquake, *Geophys. Res. Lett.,* **32**(4), doi:10.1029/2004GL021646.

Diehl, T., Waldhauser, F., Cochran, J.R., Kamesh Raju, K.A., Seeber, L., Schaff, D. & Engdahl, E.R., 2013. Back-arc extension in the Andaman Sea: tectonic and magmatic processes imaged by high-precision teleseismic double-difference earthquake relocation, *J. geophys. Res.: Solid Earth,* **118,** 2206–2224.

Djellit, H., 1987. Evolution tectono-metamorphique du socle Kabyle et polarité de mise en place des nappes de flysches en petite Kabylie occidentale (Algerie), *PhD thesis,* Univ. Paris- University, France.

Doglioni, C., Fernandez, M., Gueguen, E. & Sabat, F., 1999. On the interference between the early Apennines–Maghrebides back-arc extension and the Alps-Betics orogen in the Neogene geodynamics of the Western Mediterranean, *Bull. Soc. Geol. Ital.,* **118,** 75–89.

Domzig, A. *et al.*, 2006. Searching for the Africa-Eurasia Miocene boundary offshore western Algeria (MARADJA'03 cruise), *Compt. Rendus Géosci.,* **338**(1-2), 80–91.

Domzig, A., 2006. Déformation active et récente, et structuration tectono-sédimentaire de la marge sous-marine algérienne, *PhD thesis,* UBO University, Brest, France, 332 pp.

Dubourdieu, G., 1956. Etude géologique de la région de l'Ouenza (confins-Algéro-tunisiens) publication du service de la carte géologique de l'Algérie, Bulletin N° 10, 659 pp.

Durand-Delga, M., 1969. Mise au point sur la structure de l'Algérie septentrionale, *Bull. Serv. Carte Géol. Algérie,* **39,** 89–131.

Faccenna, C., Becker, T.W., Lucente, F.P., Jolivet, L. & Rossetti, F., 2001. History of subduction and back-arc extension in the Central Mediterranean, *Geophys. J. Int.,* **145**(3), 809–820.

Faccenna, C., Civetta, L., D'Antonio, M., Funiciello, F., Margheriti, L. & Piromallo, C., 2005. Constraints on mantle circulation around the deforming Calabrian slab, *Geophys. Res. Lett.,* (32), L06311, doi:10.1029/2004GL021874.

Fox, J.J. & Gallo, G.G., 1984. A tectonic model for ridge-transform-ridge plate boundaries: implication for the structure of oceanic lithosphere, *Tectonophysics,* **104,** 205–242.

Francis, T.J.G., 1981. Serpentinization faults and their rôle in the tectonic of slow spreading ridges, *J. geophys. Res.,* **86,** 11 616–11 622.

Frizon de Lamotte, D., Saint Bezar, B.A., Bracene, R. & Mercier, E., 2000. The two main steps of the Atlas building and geodynamics of the western Mediterranean, *Tectonics,* **19**(4), 740–761.

Funck, T., Jackson, H.R., Louden, K.E., Dehler, S.A. & Wu, Y., 2004. Crustal structure of the northern Nova Scotia rifted continental margin (eastern Canada), *J. geophys. Res.: Solid Earth,* **109**(B9), doi:10.1029/2004JB003008.

Gailler, A., Klingelhoefer, F., Olivet, J.L. & Aslanian, D. P. Sardinia Sci. & O.B.S.T. Tech., 2009. Crustal structure of a young margin pair: new results across the Liguro-rovencal Basin from wide-angle seismic tomography, *Earth planet. Sci. Lett.,* **286**(1–2), 333–345.

Galdeano, A. & Rossignol, J-C., 1977. Assemblage à altitude constante de cartes d'anomalies magnétiques couvrant l'ensemble du bassin occidental de la Méditerranée, *Bull. Soc. géol. France,* **7**, 461–468.

Gallais, F., Graindorge, D., Gütscher, M.-A. & Klaeschen, D., 2013. Propagation of a lithospheric tear fault (STEP) through the western boundary of

the Calabrian accretionary wedge offshore eastern Sicily (Southern Italy), *Tectonophysics,* **602,** 141–152.

Gattacceca, J., Deino, A., Rizzo, R., Jones, D.S., Henry, B., Beaudoin, B. & Vadeboin, F., 2007. Miocene rotation of Sardinia: new paleomagnetic and geochronological constraints and geodynamic implications, *Earth planet. Sci. Lett.,* **258,** 359–377.

Gautier, F., Clauzon, G., Suc, J.P., Cravatte, J. & Violanti, D., 1994. Age and duration of the Messinian salinity crisis, *Comptes Rendus De L'Académie Des Sciences Série II,* **318**(8), 1103–1109.

Gelabert, B., Sabat, F. & Rodriguez-Perea, A., 2002. A new proposal for the late Cenozoic geodynamic evolution of the western Mediterranean, *Terra Nova,* **14**(2), 93–100.

Géry, B., Feinberg, H., Lorenz, C. & Magné, J., 1981. Définition d'une série type de « l'Oligo-miocène Kabyle » anté-nappes dans le Djebel Aissa-Mimoun (grande Kabylie, Algérie), *C.R. Acad. Sci. Paris,* **292,** 1529–1532.

Govers, R. & Wortel, M.J.R., 2005. Lithosphere tearing at STEP faults: response to edges of subduction zones, *Earth planet. Sci. Lett.,* 505–523.

Grad, M. & Tiira, T. ESC Working Group, 2009. The Moho depth map of the European Plate, *Geophys. J. Int.,* **176,** 279–292.

Grevemeyer, I., Ranero, C., Leuchters, W., Pesquer, D., Booth-Rea, G. & Gallart, J., 2011. Seismic constraints on the nature of crust in the Algerian-Balearic basin—implications for lithospheric construction at back-arc spreading centres, *EOS, Trans., Am. geophys. Un.*, Abstract T53D-04.

Grevemeyer, I., Weigel, W., Whitmarsh, R.B., Avedik, F. & Dehghani, G.A., 1997. The Aegir Rift: crustal structure of an extinct spreading axis, *Mar. geophys. Res.,* **19,** 1–23.

Gueguen, E., Doglioni, C. & Fernander, M., 1998. On the post-25 Ma geodynamic evolution of the western Mediterranean, *Tectonophysics,* **298,** 259–269.

Hilly, J., 1962. Etude géologique du massif de l'Edough et du cap de fer (Est-constantinois). Publication de la carte géologique de l'Algérie, Bulletin N°19, 408 pp.

Hinz, K., 1973. Crustal structure of Balearic Sea, *Tectonophysics,* **20**(1–4), 295–302.

Horen, H., Zamora, M. & Dubuisson, G., 1996. Seismic waves velocities and anisotropy in serpentinized peridotites from Xigaze ophiolite: abundance of serpentine in slow spreading ridge, *Geophys. Res. Lett.,* **23**(1), 9–12.

Jackson, H.R., Reid, I. & Falconer, R.K.H., 1982. Crustal structure near the Arctic Mid-Ocean Ridge, *J. geophys. Res.,* **87**(B3), 1773–1783.

Jallouli, C., Chikhaoui, M., Braham, A., Turki, M.M., Mickus, K. & Benassi, R., 2005. Evidence for Triassic salt domes in the Tunisian Atlas from gravity and geological data, *Tectonophysics,* **396,** 209–225.

Jokat, W. & Schmidt Aursch, M.C., 2007. Geophysical characteristics of the ultraslow spreading Gakkel Ridge, Arctic Ocean, *Geophys. J. Int.,* **168**(3), 983–998.

Jolivet, L. & Faccenna, C., 2000. Mediterranean extension and the Africa-Eurasia collision, *Tectonics,* **19**(6), 1095–1106.

Jolivet, L., Faccenna, C., Goffé, B., Burov, E. & Agard, P., 2003. Subduction tectonics and exhumation of high pressure metamorphic rocks in the Mediterranean orogens, *Am. J. Sci.,* **303,** 353–409.

Karig, D. & Jensky, W., 1972. The proto-Gulf of California, *Earth planet. Sc. Lett.,* **17,** 169–174.

Karson, J.A., Collins, J.A. & Casey, J.F., 1984. Geologic and seismic velocity structure of the crust/mantle transition in the Bay of Islands ophiolite complex, *J. geophys. Res.,* **89**(B7), 6126–6138.

Keskin, M., 2003. Magma generation by slab steepening and breakoff beneath a subduction-accretion complex: an alternative model for collision-related volcanism in Eastern Anatolia, Turkey, *Geophys. Res. Lett.,* **30**(24), 8046–8059.

Kherroubi, A. *et al.*, 2009. Recent and active deformation pattern off the easternmost Algerian margin, Western Mediterranean Sea: new evidence for contractional tectonic reactivation, *Mar. Geol.,* **261**(1–4), 17–32.

Klingelhoefer, F. & Géli, L., 2000. Geophysical and geochemical constraints on crustal accretion at the very-slow spreading Mohns Ridge, *Geophys. Res. Lett.,* **27**(10), 1547–1550.

Klingelhoefer, F., Géli, L., Matias, L., Steinsland, N. & Mohr, J., 2000. Crustal structure of a superslow spreading centre: a seismic refraction study of Mohns Ridge, 72° N, *Geophys. J. Int.,* **141,** 509–526.

Klingelhoefer, F., Edwards, R.A., Hobbs, R.W. & England, R.W., 2005. Crustal structure of the NE Rockall Trough from wide-angle seismic data modeling, *J. geophys. Res.: Solid Earth,* **110**(B11), doi:10.1029/2005JB003763.

Klingelhoefer, F. *et al.*, 2008. Preliminary results from the SARDINIA deep seismic cruise on the Western Sardinia and Gulf of Lions conjugate margin pair, in *EGU Meeting April 2008,* Vienna.

Kokinou, E., Alves, T. & Kamberis, E., 2012. Structural decoupling in a convergent forearc setting (southern Crete, Eastern Mediterranean), *Geol. Soc. Am. Bull.,* **124,** 1352–1364.

Korenaga, J., Holbrook, W.S., Kent, G.M., Kelemen, P.B., Detrick, R.S. & Larsen, H.C., 2000. Crustal structure of the southeast Greenland margin from joint refraction and reflection seismic tomography, *J. geophys. Res.,* **105**(B9), 21 591–21 614.

Krijgsman, W., Hilgen, F.J., Raffi, I., Sierro, F.J. & Wilson, D.S., 1999. Chronology, causes and progression of the Messinian salinity crisis, *Nature,* **400**(6745), 652–655.

Laouar, R., Boyce, A.J., Ahmed-Said, Y., Ouabadi, A., Fallick, A.-E. & Toubal, A., 2002. Stable isotope study of the igneous, metamorphic and mineralized rocks of the Edough complex, Annaba, Northeast Algeria, *J. Afr. Earth Sci.,* **35,** 271–283.

Laouar, R., Boyce, A.J., Arafa, M., Ouabadi, A. & Fallick, A.E., 2005. Petrological, geochemical, and stable isotope constraints on the genesis of the Miocene igneous rocks of Chetaibi and Cap de Fer (NE Algeria), *J. Afr. Earth Sci.,* **41,** 445–465.

Lelgemann, H. & Klaeschen, D., 1999. AVA analysis in the eastern Mediterranean, *Phys. Chem. Earth, Part A: Solid Earth Geod.,* **24,** 467–474.

Leprêtre, A., Klingelhoefer, F., Graindorge, D., Schnurle, P., Beslier, M.O., Yelles, K., Déverchère, J. & Bracene, R., 2013. Multiphased tectonic evolution of the Central Algerian margin from combined wide-angle and reflection seismic data off Tipaza, Algeria, *J. geophys. Res.: Solid Earth,* **118,** 1–18.

Lofi, J. *et al.*, 2011a. Seismic Atlas of the Messinian Salinity Crisis markers in the Mediterranean and Black Seas, pp. 1–72, 1 CD Projet GDR Marges "Eclipses", Actions Marges, Total, BRGM.

Lofi, J. *et al.*, 2011b. Refining our knowledge of the Messinian salinity crisis records in the offshore domain through multi-site seismic analysis, *Bull. Soc. Géol. de France,* **182**(2), 163–180.

Lonergan, L. & White, N., 1997. Origin of the Betic-Rif mountain belt, *Tectonics,* **16**(3), 504–522.

Lustrino, M., Duggen, S. & Rosenberg, C.L., 2011. The Central-Western Mediterranean: anomalous igneous activity in an anomalous collisional tectonic setting, *Earth-Sci. Rev.,* **104,** 1–40.

Malinverno, A. & Ryan, W.B.F., 1986. Extension in the Tyrrhenian sea and shortening in the Apennnines as result of the arc migration driven by sinking of the lithosphere, *Tectonics,* **5,** 227–245.

Mantovani, E., Cenni, N., Albarello, D., Viti, M., Babbucci, D., Tamburelli, C. & D'Onza, F., 2001. Numerical simulation of the observed starin field in the central-eastern Mediterranean region, *J. Geodyn.,* **31,** 519–556.

Marsellos, A.E., Kidd, W.S.F. & Garver, J.L., 2010. Extension and exhumation of the HP/LT rocks in the Hellenic fore-arc ridge, *Am. J. Sci.,* **310,** 1–36.

Martin, A.K., 2006. Oppositely directed pairs of propagating rifts in back-arc basins: double saloon door seafloor spreading during subduction rollback, *Tectonics,* **25,** TC3008, doi:10.1029/2005TC001885.

Mascle, G.H. *et al.*, 2004. Structure of the Sardinia Channel: crustal thinning and tardi-orogenic extension in the Apenninic-Maghrebian orogen; results of the Cyana submersible survey (SARCYA and SARTUCYA) in the western Mediterranean, *Bull. Soc. géol. Fr.,* **175**(6), 607–627.

Mauffret, A., 2007. The Northwestrn (Maghreb) Boundary of the Nubia (Africa) Plate, *Tectonophysics,* **429,** 21–44.

Mauffret, A., Frizon de Lamotte, D., Lallemant, S., Gorini, C. & Maillard, A., 2004. E-W opening of the Algerian basin (Western Mediterranean), *Terra Nova,* **16**(5), 257–264.

Maury, R.C. *et al.*, 2000. Post-collision neogene magmatism of the Mediterranean Maghreb margin: a consequence of slab breakoff, *C.R. Acad. Sci. Paris,* **331,** 159–173.

Medaouri, M., Déverchère, J., Graindorge, D., Bracene, R., Badji, R., Ouabadi, A., Yelles, K. & Bendib, F., 2014. The transition from Alboran to Algerian basins (Western Mediterranean Sea): chronostratigraphy, deep crustal structure and tectonic evolution at the rear of a narrow slab rollback system, *J. Geodyn.,* **77,** 186–205.

Michard, A., Negro, F., Saddiqi, O., Bouybaouene, M.L., Chalouan, A., Montigny, R. & Goffé, B., 2006. Pressure-temperature-time constraints on the Maghrebide mountain building: evidence from the Rif-Betic transect (Morocco, Spain), Algerian correlations, and geodynamic implications, *C. R. Geosci.,* **338,** 92–114.

Mihoubi, A. *et al.*, 2014. Seismic imaging of the eastern Algerian margin off Jijel: integrating wide-angle seismic modeling and multichannel seismic pre-stack depth migration, *Geophys. J. Int.,* **198,** 1486–1503.

Miller, D.J. & Christensen, N.I., 1997. Seismic velocities of lower crustal and upper mantle rocks from the slow spreading Mid-Atlantic Ridge, south of the Kane Transformation Zone (MARK), in *Proceedings of the Ocean Drilling Program, Scientific Results,* Vol. 153, pp. 437–451, eds Karson, J.A., Cannat, M., Miller, D.J. & Ethon, D., College Station, TX (Ocean Drilling Program).

Minshull, T.A. & White, R.S., 1996. Thin crust on the flanks of the slow-spreading Southwest Indian Ridge, *Geophys. J. Int.,* **125,** 139–148.

Minshull, T.A., White, R.S., Mutter, J.C., Buhl, P., Detrick, R.S., Williams, C.A. & Morris, E., 1991. Crustal structure at the Blacks Spur Fracture Zone from expanding spread profiles, *J. geophys. Res.,* **96,** 9955–9984.

Monié, P., Caby, R. & Maluski, H., 1984. 40Ar/39Ar investigations within the Grande-Kabylie Massif (northern Algeria): evidences for its Alpine structuration, *Eclog. Geol. Helv.,* **77,** 115–141.

Newman, P., 1973. Divergence effects in a layered Earth, *Geophysics,* **38,** 481–488.

Nicholls, I.A., Ferguson, J., Jones, H., Marks, G.P. & Mutter, J.C., 1981. Ultramafic blocks from the océan floor southwest of Australia, *Earth planet. Sci. Lett.,* **56,** 362–374.

Ogilvie, J.S. & Purnell, G.W., 1996. Effects of salt-related mode conversions on subsalt prospecting, *Geophysics,* **61**(2), 331–348.

Palomeras, I., Thurner, S., Levander, A. & Liu, K., 2014. Finite-frequency Rayleigh wave tomography of the western Mediterranean: mapping its lithospheric structure, *Geochem. Geophys. Geosyst.,* **15,** 140–160.

Peirce, C. & Barton, P.J., 1992. Southern Segment of the European Geotraverse—a wide-angle refraction survey in the Sardinia Channel, *Mar. Geophys. Res.,* **14,** 227–248.

Pertthuisot, V. & Rouvier, H., 1992. Les diapirs du Maghreb central et oriental : des diapirs variés, résultats d'une évolution structurale et pétrogénétique complexe, *Bull, soc, géol, France,* **163**(6), 751–760.

Piromallo, C. & Morelli, A., 2003. P wave tomography of the mantle under the Alpine-Mediterranean area, *J. geophys. Res.,* **108**(B2), 2065, doi:10.1029/2002JB001757.

Potts, C.G., Whitev, R.S. & Louden, K.E., 1986. Crustal structure of Atlantic fracture zones II: the Vema fracture zone and transverse ridge, *Geophys. J. R.. astr. Soc.,* **86,** 491–513.

Prada, M., Sallares, V., Ranero, C.R. & Vendrell, G., 2014. Seismic structure of the Central Tyrrhenian basin: geophysical constrains on the nature of the main crustal domains, *J. geophys. Res.: Solid Earth,* **119,** 1–19.

Price, C. & Morgan, J., 2000. Lithospheric structure of Scotland-II Poisson's ratios and waveform modelling, *Geophys. J. Int.,* **142,** 737–754.

Purdy, G.M., 1983. The seismic structure of 140 Myr old crust in the western central Atlantic Ocean, *Geophys. J. R. astr. Soc.,* **72,** 115–137.

Réhault, J.-P., Boillot, G. & Mauffret, A., 1984. The Western Mediterranean Basin geological evolution, *Mar. Geol.,* **55,** 445–475.

Rivière, M., Bouillin, J.P., Courtois, C., Gélard, J.P. & Raoult, J.F., 1977. Etude minéralogique et géochimique des tuffites découvertes dans l'Oligo-Miocène kabyle (Grande Kabylie, Algérie). Comparaison avec les tuffites de la région de Malaga (Espagne), in *Bull. Soc. Géol. France,* Série 7, T. XIX, N°5, pp. 1171–1177.

Rodkin, M.V. & Rodnikov, A.G., 1996. Origin and structure of back-arc basins: new data and model discussion, *Phys. Earth planet. Int.,* **93,** 123–131.

Rollet, N., Déverchère, J., Beslier, M.O., Guennoc, P., Rehault, J.P., Sosson, M. & Truffert, C., 2002. Back arc extension, tectonic inheritance, and volcanism in the Ligurian Sea, Western Mediterranean, *Tectonics,* **21**(3), doi:10.1029/2001TC900027.

Rosenbaum, G., Gasparon, M., Lucente, F.P., Peccerillo, A. & Miller, M.S., 2008. Kinematics of slab tear faults during subduction segmentation and implications for Italian magmatism, *Tectonics*, **27**(2), doi:10.1029/2007TC002143.

Rosenbaum, G. & Lister, G.S., 2004a. Neogene and Quaternary rollback evolution of the Tyrrhenian Sea, the Apennines, and the Sicilian Maghrebides, *Tectonics,* **23**(1), doi:10.1029/2003TC001518.

Rosenbaum, G. & Lister, G.S., 2004b. Formation of arcuate orogenic belts in the western Mediterranean region, *Geol. Soc. Am., Special Papers,* **383,** 41–56.

Rosenbaum, G., Lister, G.S. & Duboz, C., 2002. Reconstruction of the tectonic evolution of the western Mediterranean since the Oligocene, in: Rosenbaum, G. & Lister, G.S. 2002—reconstruction of the evolution of the Alpine-Himalayan Orogen, *J. Virtual Explor.,* **8,** 107–126.

Roure, F., Casero, P. & Addoum, B., 2012. Alpine inversion of the North African margin and delamination of its continental lithosphere, *Tectonics,* **31,** TC3006, doi:10.1029/2011TC002989.

Rouvier, H., 1977. Géologie de l'extrême Nord tunisien: tectoniques et paléogéographies superposées à l'extrémité orientale de la chaîne nord-maghrébine, *PhD thesis,* Pierre et Marie Curie University, Paris, France, 898 pp.

Royden, L.H., 1993. The tectonic expression of slab pull at continental convergent boundaries, *Tectonics,* **12,** 303–325.

Saadallah, A. & Caby, R., 1996. Alpine extensional detachment tectonics in the Grande Kabylie metamorphic core complex of the Maghrebides (northern Algeria), *Tectonophysics,* **267,** 257–273.

Sage, F. *et al.*, 2011. Structure and evolution of a passive margin in a compressive environment: example of the south-western Alps-Ligurian basin junction during the Cenozoic, *Mar. Petrol. Geol.,* **28,** 1263–1282.

Sage, F., Pontoise, B., Mascale, J. & Basile, C., 1997. Structure of oceanic crust adjacent to as transform margin segment: the Côte d'Ivoire-Ghana transform margin, *Geo-Mar. Lett.,* **17,** 31–39.

Sartori, R., Carraraa, G., Torelli, L. & Zitellini, N., 2001. Neogene evolution of the southwestern Tyrrhenian Sea (Sardinia Basin and western Bathyal plain), *Mar. Geol.,* **175,** 47–66.

Schettino, A. & Turco, E., 2006. Plate kinematics of theWestern Mediterranean region during the Oligocene and Early Miocene, *Geophys. J. Int.,* **166**(3), 1398–1423.

Spakman, W. & Wortel, M.J.R., 2004. A tomographic view on Western Mediterranean Geodynamics, in *The TRANSMED Atlas: The Mediterranean Region from Crust to Mantle,* pp. 31–52, eds Cavazza, W., Roure, F., Spakman, W., Stampfli, GM. & Ziegler, P., Springer-Verlag.

Spakman, W., van der Lee, S. & van der Hilst, R., 1993. Travel-time tomography of the European Mediterranean mantle down to 1400 km, *Phys. Earth planet. Inter.,* **79**(1–2), 3–74.

Spudish, P. & Orcutt, J.A., 1980. A new look at the seismic velocity structure of oceanic crust, *Res. Geophys.,* **18,** 627–645.

Stockwell, J.W., 1999. The CWP/SU: seismic unix package, *Comput. Geosci.* **25**(4), 415–419.

Tapponnier, P., Peltzer, G. & Armijo, R., 1986. On the mechanics of the collision between India and Asia, in *Collision Tectonics,* Vol. 19, pp. 115–157, eds Coward, M.P. & Ries, A.C., Geol. Soc. Spec. Publ.

Ten Veen, J.H. & Kleinspehn, K.L., 2003. Incipient continental collision and plate boundary curvature: late Pliocene-Holocene transtensuinal Hellenic forearc, Crete, Greece, *J. Geol. Soc., Lond.,* **160,** 161–181.

Thurner, S., Palomeras, I., Levander, A., Carbonell, R. & Lee, C.-T., 2014. Ongoing lithospheric removal in the western Mediterranean: evidence from Ps receiver functions and thermobarometry of Neogene basalts (PICASSO project), *Geochem. Geophys. Geosyst.,* **15,** 1113–1127.

Tricart, P., Torelli, L., Argnani, A., Rekhiss, F. & Zitellini, N., 1994. Extensional collapse related to compressional uplift in the Alpine Chain off northern Tunisia (Central Mediterranean), *Tectonophysics,* **238,** 317–329.

Van Avendonk, H.J.A., Holbrook, W.S., Nunes, G.T., Shillington, D.J., Tucholke, B.E., Louden, K.E., Larsen, H.C. & Hopper, J.R., 2006. Seismic velocity structure of the rifted margin of the eastern Grand Banks of Newfoundland, Canada, *J. geophys. Res.,* **111,** B11404, doi:10.1029/2005JB004156.

Van Hinsbergen, D.J.J., Vissers, R.L.M. & Spakman, W., 2014. Origin and consequences of western Mediterranean subduction, rollback, and slab segmentation, *Tectonics,* **33,** 393–419.

Vergés, J. & Fernàndez, M., 2012. Tethys–Atlantic interaction along the Iberia–Africa plate boundary: the Betic–Rif orogenic system, *Tectonophysics,* **579,** 144–172.

Vergés, J. & Sabàt, F., 1999. Constraints on the Western Mediterranean kinematics evolution along a 1000-km transect from Iberia to Africa, in *The Mediterranean Basin: Tertiary Extensions within the Alpine Orogen,* Vol. 156, pp. 63–80, eds Durand, B., Jolivet, L., Horvath, F. & Séranne, M., Geol. Soc. Spec. Publ.

Vidal, N., Gallart, J. & Danobeitia, J.J., 1998. A deep seismic crustal transect from the NE Iberian Peninsula to the Western Mediterranean, *J. geophys. Res.: Solid Earth,* **103**(B6), 12 381–12 396.

Vila, J.M., 1978. Carte structurale au 1/50.000 de la chaîne alpine d'Algérie orientale et des confins Algéro-Tunisiens. Service de cartes géologiques, Algérie/Sonatrach.

Vila, J.M., 1980. La chaine alpine d'Algérie orientale et des confins Algéro-Tunisien, *PhD Thesis,* Univ. Pierre et Marie Curie (Paris VI), France, 665 pp.

White, R.S. & Stephen, R.A., 1980. Compressional to shear wave conversion in oceanic crust, *Geophys. J. R. astr. Soc.,* **63,** 541–565.

Wessel, P. & Smith, W.H.F., 1995. New version of the generic mapping tools released, *EOS, Trans. Am. geophys. Un.,* **76**(33), 329, doi:10.1029/95EO00198.

White, R.S., Detrick, R.S., Sinha, M.C. & Cormier, M.H., 1984. Anomalously seismic crustal structure of oceanic fracture zones, *Geophys. J. R. astr. Soc.,* **79,** 779–798.

White, R.S., McKenzie, D. & Onions, R.K., 1992. Oceanic crustal thickness from seismic measurements and rare-earth element inversions, *J. geophys. Res.: Solid Earth,* **97**(B13), 19 683–19 715.

Whitmarsh, R.B. & Miles, P.R., 1995. Models of the development of the West Iberia rifted continental-margin at 40 degrees 30′N deduced from surface and deep-tow magnetic-anomalies, *J. geophys. Res.: Solid Earth,* **100**(B3), 3789–3806.

Whitmarsh, R.B., White, R.S., Horsefield, S.J., Sibuet, J.C., Recq, M. & Louvel, V., 1996. The ocean-continent boundary off the western continental margin of Iberia: crustal structure west of Galicia Bank, *J. geophys. Res.: Solid Earth,* **101**(B12), 28 291–28 314.

Wildi, W., 1983. La chaîne tello rifaine (Algérie, Maroc, Tunisie): structure, stratigraphie et évolution du Trias au Miocène, *Rev. Géol. Dyn. géog. Phys.,* **3**(24), 201–297.

Wortel, M.J.R. & Spakman, W., 2000. Subduction and slab detachment in the Mediterranean-Carpathian region, *Sciences,* **290,** 1910–1917.

Yelles, A. *et al.*, 2009. Plio-Quaternary reactivation of the Neogene margin off NW Algiers, Algeria: the Khayr al Din bank, *Tectonophysics,* **475**(1), 98–116.

Zelt, C.A., 1999. Modelling strategies and model assessment for wide-angle seismic traveltime data, *Geophys. J. Int.,* **139,** 183–204.

Zelt, C.A. & Smith, R.B., 1992. Seismic traveltime inversion for 2-D crustal velocity structure, *Geophys. J. Int.,* **108,** 16–34.